



Specific adsorbents for the treatment of OMW phenolic compounds by activation of bio-residues from the olive oil industry

Bruno M. Esteves^a, Sergio Morales-Torres^b, Luis M. Madeira^a, Francisco J. Maldonado-Hódar^{b,*}

^a LEPABE – Laboratory for Process Engineering, Environment, Biotechnology and Energy, Faculty of Engineering, University of Porto, Rua Dr. Roberto Frias, 4200-465, Porto, Portugal

^b NanoTech – Nanomaterials and Sustainable Chemical Technologies, Department of Inorganic Chemistry, Faculty of Sciences, University of Granada, Avda. Fuente Nueva, 18071, Granada, Spain

ARTICLE INFO

Keywords:

Activated carbon
Biosorbent
Phenolic acid
Wastewater treatment
Adsorption
Olive mill wastewater

ABSTRACT

A series of adsorbents was developed by physical (CO₂) and chemical (KOH) activation of two bio-residues: olive stones (OS) and wood from olive tree pruning (OTP). The physicochemical properties of such materials were determined and correlated with their adsorptive performance in the removal of phenolic compounds of olive mill wastewater (OMW). Adsorption isotherms and kinetics of single phenolic acids, as well as the kinetics for competitive multi-compound adsorption, were fitted by applying different models, though Langmuir and pseudo-second order models fitted better the experimental results, respectively. The intraparticle diffusion model pointed out that mesoporosity reduces the influence of phenolic compounds' restrictions in the external film diffusion of the adsorbent particle–solution interphase, but adsorption capacity linearly increases with the micropore volume accessible to N₂ at –196 °C (and also with BET surface area), while diffusion into ultramicropores (<0.7 nm, determined by CO₂-adsorption) is slow and presents minor influence on the total adsorption capacity. After saturation, thermal regeneration of spent adsorbents allows the removal of adsorbed products, enabling the reuse of samples whilst maintaining a significant performance.

1. Introduction

The olive oil industry is a strategic sector for many countries around the world, particularly in the Mediterranean region, where the local heritage of production, consumption, and trade of olive oil has historical socio-economic importance. However, olive oil extraction can also entail several adverse environmental impacts, mainly related to the simultaneous generation of large volumes of olive mill wastewater (OMW) containing different types of pollutants. OMW typically presents high phytotoxicity, high organic load (chemical oxygen demand, COD), low pH, strong dark-brown coloration, and involves the generation of unpleasant odorous gases (Niaounakis and Halvadakis, 2006; Paraskeva and Diamadopoulos, 2006). Several organic contaminants present in OMW, particularly the polyphenolic fraction, fats, and lipids, are non-biodegradable and therefore with persistent toxicity in solution (Fajardo et al., 2015; Justino et al., 2009). Different techniques have been proposed for the management of OMW, including those based on the destruction (e.g. advanced oxidative processes, AOPs (Ochando-Pulido et al., 2017; Kilic et al., 2019)), concentration by adsorption

(Frasconi et al., 2016; Stasinakis et al., 2008), separation/recovery by membranes (Ochando-Pulido et al., 2020; Stoller et al., 2016; Garcia-Castello et al., 2010), ion exchange resins (Zagklis et al., 2015; Victor-Ortega et al., 2016), or solvent extraction (Dermeche et al., 2013) of valuable substances present in solution.

Adsorption processes are a potential approach for the removal of phenolic compounds from OMW, mainly due to the processes' simplicity of design, operation, and scale-up (Soto et al., 2011). Nevertheless, the much higher COD values of OMW (up to 200 g/L) in comparison to the average range for total phenolic content (up to 7.5 g/L) (Ochando-Pulido et al., 2017), may hinder phenolic compounds' adsorption by competition with different components in solution (e.g., tannins, sugars, organic acids) due to differences in concentration, molecular size and affinity towards the adsorbent (Al-Malah et al., 2000). The development of low-cost porous adsorbents with high specificity for phenols contained in OMW is therefore mandatory for this application. Biomass-derived activated carbon (AC) materials emerged as a clear and cheap alternative to commercial adsorbents (zeolites, inorganic oxides, MOFs, etc. (Ahmaruzzaman, 2008)), thanks to the wide availability of such by-products from a wide range of industrial activities (Jeguirim

* Corresponding author.

E-mail address: fjaldon@ugr.es (F.J. Maldonado-Hódar).

List of acronyms and abbreviations

AC	Activated carbon
AOP	Advanced oxidation process
BET	Brunauer–Emmett–Teller
CA	Caffeic acid
COD	Chemical oxygen demand
DLD	Delay-line detector
EDX	Energy-dispersive X-ray
GA	Gallic acid
HPLC	High-performance liquid chromatography
HRSEM	High-resolution scanning electron microscopy
MOF	Metal-organic framework
MSC	Mathematical/model selection criterion
N	Norit RX-3 Extra
OMW	Olive mill wastewater
OS	Olive stone
OSAC	Olive stone activated carbon
OSG	Oxygenated surface groups
OTP	Olive tree pruning
OTPAC	Olive tree pruning activated carbon
PA	Protocatechuic acid
pH _{pzc}	pH at the point of zero charge
PFO	Pseudo-first order
PSD	Pore size distribution
PSO	Pseudo-second order
PTFE	Polytetrafluoroethylene

QSDFT	Quenched solid density functional theory
RMSE	Root mean square error
TG/DTG	Thermogravimetry/Derivative thermogravimetry
TPh	Total phenolic content
TY	Tyrosol
VA	Vanillic acid
XPS	X-ray photoelectron spectroscopy

List of Variables

C_0	Initial concentration (mg/L)
C_e	Equilibrium concentration (mg/L)
h	Initial adsorption rate (mg/gmin)
k_1	Pseudo-first order rate constant (1/min)
k_2	Pseudo-second order rate constant (g/mg min)
K_F	Freundlich constant ((mg/g)(mg/L) ⁿ)
K_{id}	Intraparticle diffusion rate constant (mg/g min ^{1/2})
K_L	Langmuir constant (L/mg)
L_0	Mean micropore width (nm)
q_e	Equilibrium adsorption capacity (mg/g)
q_m	Maximum adsorption capacity (mg/g)
S_{BET}	BET surface area (m ² /g)
V_{meso}	Volume of mesopores (cm ³ /g)
V	Volume (L)
V_T	Total pore volume (cm ³ /g)
W_0	Volume of micropores (cm ³ /g)
W_{ads}	Adsorbent mass (g)

et al., 2018). The use of organic residues from the olive oil extraction industry, either as biosorbents or as precursors for their preparation, has already been described in the literature. Many authors reported on the purification of effluents containing heavy metals (e.g., Pb²⁺, Cu²⁺, Fe³⁺, Cr⁶⁺) using ACs prepared from exhausted olive-waste cakes (Baccar et al., 2009), from olive peel and seed (Petrella et al., 2018), or even raw olive stones (Hodaifa et al., 2013). The adsorption of different organic pollutants by similar biosorbents was also already reported, including ACs prepared from olive stones (Hazzaa and Hussein, 2015) and olive-waste cakes (Baccar et al., 2010) for dye removal, biosorption of phenolic compounds with solvent-washed olive wood (El-Sheikh et al., 2013), solvent-extracted olive husks (Stasinakis et al., 2008), and AC-derived olive husks (Michailof et al., 2008), as well as ACs prepared from olive stones and solvent-extracted olive pulp (Galiatsatou et al., 2002).

In this study, porous ACs prepared from olive stone (OS) and olive tree pruning (OTP) were synthesized by physical and chemical activation processes and tested for the adsorption of several phenolic compounds typically found in real OMW. The combination of different residues and activation processes to produce bio-carbons with different physicochemical properties, along with the knowledge of the relationship of these parameters with the adsorption performances, will favor the development of cheap and specific adsorbents suitable for phenolic effluent's treatment. This approach allows the revalorization of residues within this industry, the appropriate treatment of OMW by environmentally friendly processes, the potential recovery of valuable substances and reuse of water, in line with the circular economy trend.

2. Materials and methods

2.1. Synthesis of materials

Olive stone and olive tree pruning were selected as precursors for the synthesis of physically activated carbons. The raw agricultural waste was first washed thoroughly, then ground and sieved to a particle size

fraction of 0.45–0.80 mm. Samples were prepared by a two-step process in a horizontal tube furnace: first, the carbonization of raw materials was carried out at 800 °C (10 °C/min heat ramp, 2 h hold time) in a 150 cm³/min N₂ flow (volumetric flow rates reported at ambient temperature and atmospheric pressure), followed by physical activation by switching the flow of N₂ to CO₂ (300 cm³/min, 4 h); after that time, the flow is again switched to N₂, the oven turned off, and the samples allowed to reach room temperature (Baçaoui et al., 2002). The derived ACs were denoted as OSAC and OTPAC, corresponding to physically-activated carbons from olive stones and olive tree pruning, respectively.

Additionally, a chemically-activated sample of OS was prepared using concentrated potassium hydroxide as the activating agent. Chemical activation with KOH was carried out in one step procedure with a fraction of OS previously carbonized as described earlier, in a weight proportion of 1:1 (50% KOH: 50% OS). KOH was dissolved in the minimum amount of water and mechanically agitated with the OS-derived sample. After drying in an oven at 110 °C overnight to remove water, the OS/KOH mixture was directly heated at 800 °C for 2 h (N₂ flow, 150 cm³/min). After that, the oven was turned off and the sample cooled to room temperature in the same N₂ flow. The sample (designated OSAC/KOH) was treated in an acidic media (HCl) to remove the remaining KOH, and then washed with distilled H₂O until no chlorine ions were detected in the washing waters (adding drops of concentrated AgNO₃ solution until absence of AgCl precipitate) (Morales-Torres et al., 2010a). For comparison purposes, a commercially available high-purity steam-activated activated carbon (Norit® RX-3 Extra, from Sigma-Aldrich) was also used in this study (herein denoted as N). Prior to use, all materials were ground and sieved to powder.

2.2. Characterization of the adsorbents

The textural characterization was carried out by physical adsorption of N₂ and CO₂ at –196 °C and 0 °C, respectively, using a Quantachrome Quadrasorb SI equipment; samples were degasified for 12 h (at 120 °C)

before analysis. The Brunauer–Emmett–Teller (BET) equation was applied to N₂ adsorption isotherms (at $P/P_0 < 0.10$) to obtain the apparent surface area (S_{BET}) of the materials (Brunauer et al., 1938). Micropore volume (W_0) and mean micropore width (L_0) were determined by the Dubinin–Radushkevich and Stoeckli equations, respectively (Bansal et al., 1998; Stoeckli et al., 2002). The total pore volume (V_T) was considered as the volume of N₂ adsorbed at $P/P_0 = 0.95$, and the mesopore volume (V_{meso}) obtained from the difference between V_T and the volume of N₂ adsorbed at $P/P_0 = 0.40$, following Gurvich's rule (Rouquerol et al., 2013). The pore size distribution (PSD) was derived from the quenched solid density functional theory (QSDFT) method applied to N₂ isotherms and assuming slit-shaped pores (Neimark et al., 2009).

The morphology of the carbonaceous materials was analyzed by high-resolution scanning electron microscopy (HRSEM) using a LEO (Carl Zeiss) GEMINI-1530 microscope, equipped with an energy dispersive X-ray (EDX) microanalysis system (Oxford Instruments). Chemical characterization was performed by X-ray photoelectron spectroscopy (XPS) using a Kratos Axis Ultra-DLD apparatus; survey and multi-region spectra were recorded at C1s and O1s photoelectron peaks and each spectral region scanned until good signal-to-noise ratios were achieved. Adsorbent's pH_{pzc} (pH at the point of zero charge) values were also determined, following a previously published methodology (Newcombe et al., 1993).

2.3. Adsorbates and adsorption runs

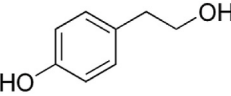
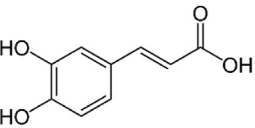
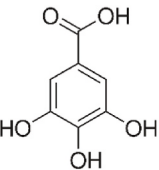
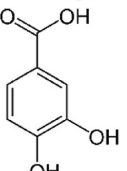
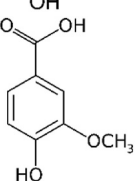
Due to the complexity and variability of the OMW characteristics, a polyphenolic synthetic solution was prepared using pure reagents, thus allowing an analysis of the interactions between phenolic compounds typically present in OMW with the prepared ACs. For this, five phenolic compounds commonly found in real OMW were selected (Aggoun et al., 2016; El-Abbassi et al., 2012; Kapellakis et al., 2008), and in

concentrations similar to those reported by some authors (De Marco et al., 2007; Tundis et al., 2021): tyrosol and vanillic acid (Sigma-Aldrich), protocatechuic and caffeic acids (ACROS Organics), and gallic acid (Alfa Aesar); their chemical structure and main characteristics are listed in Table 1. The solution was prepared by dissolving 30 mg/L of each compound in distilled water (thus yielding a total of 150 mg/L, which was also the concentration employed when using a single compound), ensuring full dissolution with the aid of an ultrasound apparatus (Argo Lab, mod. DU 45). Adsorption experiments were performed in triplicate in a 300 mL-capacity cylindrical jacketed batch reactor, under magnetic agitation at 300 rpm (VWR VS-CT magnetic stirrer) and controlled temperature ($T = 25\text{ }^\circ\text{C}$), recycling water through a model 89, 202-912 VWR International thermostatic bath. The reactor was initially loaded with 150 mL of the synthetic effluent (total phenolic content, TPh, 150 mg/L and $pH_0 \approx 3.8$) and the adsorbent sample (0.5 g/L) in powder form. This synthetic solution was used to evaluate competitive adsorption processes by following the concentration of each specific compound.

Determination of individual phenolic compounds' concentration was performed by high-performance liquid chromatography (HPLC), using a Hitachi Elite LaChrom apparatus equipped with an L-2310 pump, L-2200 auto-sampler, and L-2455 diode-array detector. A Purospher STAR RP-18 column (240 mm \times 4 mm, 5 μm) was used to achieve chromatographic separation. Mobile phases consisted of 70% (v/v) of ultrapure H₂O slightly acidified with orthophosphoric acid (1%, v/v), and 30% (v/v) of methanol ($\geq 99.8\%$, Fischer Chemical), at isocratic conditions. The system was operated at 50 $^\circ\text{C}$, with a volumetric flow rate of 1 mL/min and sample injection volume of 20 μL . The spectra were recorded at 240–280 nm, and standard curves for each phenolic compound were previously constructed using standard solutions with concentrations ranging from 5 to 100 mg/L.

Taking into account the different behavior observed between the different phenols of the mixture (as detailed later in Section 3.2), gallic

Table 1
Chemical characteristics of the phenolic compounds used.

Name	Chemical structure	Molecular formula	Max. linear dimension (Å)	Molecular weight (g/mol)	pKa (at 25 $^\circ\text{C}$)	Solubility in water (g/L)
Tyrosol		C ₈ H ₁₀ O ₂	7.8	138.16	10.20	25.3 (at 25 $^\circ\text{C}$)
Caffeic acid		C ₉ H ₈ O ₄	8.7	180.16	4.62	1.0 (at 22 $^\circ\text{C}$)
Gallic acid		C ₇ H ₆ O ₅	6.4	170.12	4.40	11.5 (at 25 $^\circ\text{C}$)
Protocatechuic acid		C ₇ H ₆ O ₄	6.3	154.12	4.48	18.2 (at 14 $^\circ\text{C}$)
Vanillic acid		C ₈ H ₈ O ₄	6.3	168.14	4.16	1.5 (at 14 $^\circ\text{C}$)

and vanillic acids were also selected for individual sorption studies (particularly because such phenolic compounds are very similar in molecular weight and dimensions, but presented rather distinct adsorptive behavior in the multi-compound solution). The corresponding adsorption isotherms on the different ACs were recorded by varying the initial concentration of pollutants in the aqueous solution (initial concentrations ranging from 25 to 350 mg/L). Stopped flasks containing 25 mg of each adsorbent (0.5 g/L) and 50 mL of the phenolic solution were agitated (300 rpm) in a thermostatic water bath shaker (Grant OLS 200) at a constant temperature of 25 °C. A sample of each flask was collected after 24 and 48 h, filtered using 0.45 μm PTFE syringe filters (VWR), and the equilibrium concentrations were determined by HPLC; whenever necessary, samples were diluted with ultrapure water prior to such analysis. It is important to note that the runs were prolonged up to 48 h to confirm that equilibrium was achieved; nevertheless, it was determined that 24 h of contact was sufficient in all cases (data not shown for brevity).

The equilibrium adsorption capacity of each adsorbent, q_e (mg/g_{ads}), was determined following Eq. (1), where C_0 and C_e (mg/L) are the adsorbate's initial and equilibrium concentrations, respectively, W_{ads} (g) the mass of adsorbent, and V (L) the volume of adsorbate solution. Adsorption isotherms were determined at the solution's initial pH, which ranged between 3.5 and 3.8.

$$q_e = \frac{(C_0 - C_e)}{W_{ads}} \times V \quad (1)$$

The adsorption kinetics of these individual compounds were also determined. For that, 150 mL of the phenolic solution ($C_0 = 150$ mg/L), i.e., with a similar total phenol concentration previously used for the competitive adsorption experiments for comparisons, were mixed with the adsorbents in Erlenmeyer flasks and agitated under the same conditions described previously. Samples (0.5 mL) were periodically withdrawn, filtered, and analyzed by HPLC, as previously described; the total volume withdrawn during each experiment corresponds to only 3% of the initial volume.

2.4. Regeneration studies

To check the reusability of the adsorbents, regeneration studies were performed with samples saturated with gallic or vanillic acid. To ensure full saturation of each sample, 100 mg of each adsorbent was placed in a 150 mL solution loaded with 1000 mg/L of the required phenolic acid and the solution was agitated for 48 h; after filtration, samples were dried at 105 °C and then placed in a desiccator. Thermal regeneration of spent samples was simulated by thermogravimetric analysis (TGA), performed under an N₂ inert atmosphere with a TGA-50H thermobalance. According to these results, the removal of phenolic acids from the ACs was performed by heating the saturated samples at 800 °C for 10 min (heat ramp 20 °C/min) under an inert N₂ flow. After cooling to room temperature, the regenerated samples were used in uptake adsorption

studies according to the experimental conditions reported in Section 2.3.

3. Results and discussion

3.1. Textural and chemical characterization of adsorbents

Experimental conditions for chemical and physical activation of OS and OTP bio-residues were fitted to produce a similar activation degree in all cases, with solid yields between 14 and 16 wt%. Yields within the same range were obtained by Galiatsatou et al. (2002) using physically-activated samples of olive stone and solvent extracted olive pulp, which were also progressively lower for higher carbonization/activation times. Nonetheless, the morphology of the ACs obtained depends on the precursor used, thus OTPAC is clearly a less dense material than OSAC, also containing a larger concentration of wider channels from the original wood structure, as denoted by HRSEM images (Fig. 1). Analogous morphological structures were already reported for ACs prepared from similar bio-residues, both CO₂-activated olive pomace (Ghouma et al., 2017) and KOH-activated olive stones (Alslaibi et al., 2014). From a practical point of view, due to the different morphology of the materials, the adsorptive behavior may be influenced by parameters such as the volume occupied by the sample or the possibility of floating in solution (if it is less dense than the solution itself – this was mitigated by the high agitation speed employed in the tests).

The materials' textural properties were examined by N₂ adsorption-desorption isotherms (Fig. 2a) and complemented with CO₂ adsorption isotherms to estimate the narrowest porosity (ultramicropores). In the absence of diffusional restrictions, W_0 (N₂) yields the total micropore volume, while W_0 (CO₂) estimates the narrowest microporosity (diameter <0.7 nm) (Cazorla-Amorós et al., 1998). A summary of the data is detailed in Table 2, which also includes the parameters obtained for the commercial sample N used as reference.

The porosity of the produced samples was influenced by the nature of the raw lignocellulosic residue, as depicted by HRSEM images, but also by the activation process employed. After carbonization and physical activation with CO₂, ACs obtained from both precursors – olive stone (sample OSAC) and olive tree pruning (sample OTPAC) – present similar total pore volume ($V_T = 0.39$ cm³/g) but a very distinct pore size distribution (Fig. 2b), as denoted by the different shape of their isotherms in Fig. 2a. Thus, the OTPAC isotherm corresponds to the type IV (formation of multilayer overlapping the monolayer adsorption on the mesopore walls, and thus the gradual curvature at increasing values of relative pressure, P/P_0), associated to mesoporous samples, as compared to a practically flat plateau in the isotherm of OSAC (predominantly type I), characteristic of microporous samples, as adsorption occurs primarily at very low P/P_0 due to micropores filling (Thommes et al., 2015). The higher N₂-adsorption at low P/P_0 pointed out that microporosity is favored in the case of OSAC, as already reported by Ghouma et al. (2017) during the preparation of ACs from olive pomace through different activation agents, while the marked slope of the N₂-adsorption

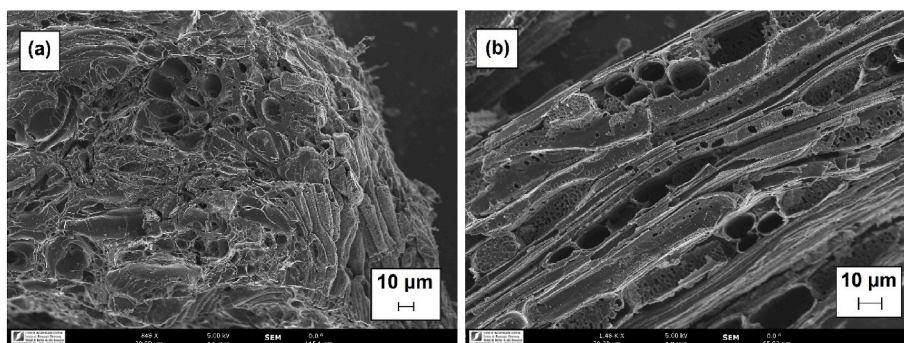


Fig. 1. HRSEM micrographs highlighting the morphology of (a) OSAC and (b) OTPAC.

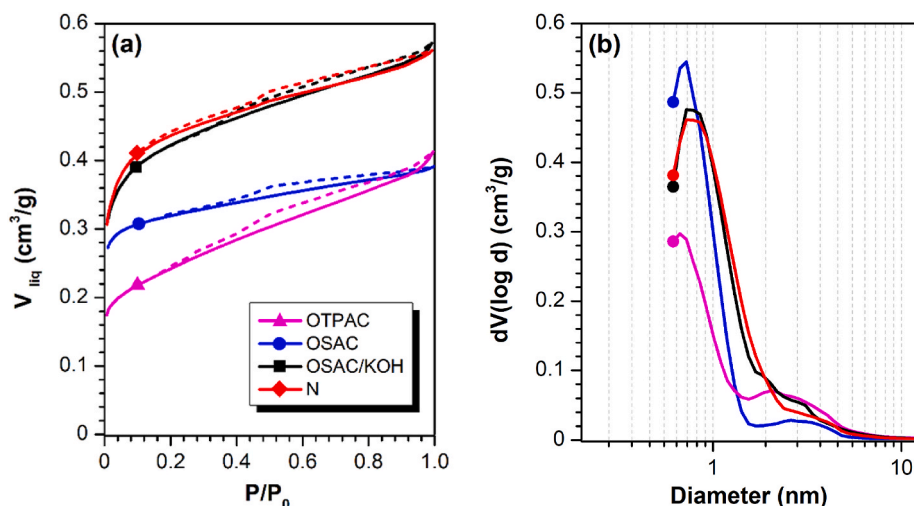


Fig. 2. (a) N_2 adsorption-desorption isotherms (P/P_0 is the relative pressure between the equilibrium pressure and the saturation vapor pressure of N_2) and (b) pore size distribution of the adsorbents.

Table 2

Textural characteristics and pH_{pzc} of the adsorbents.

Sample	S_{BET} (m^2/g)	W_0 (N_2) (cm^3/g)	L_0 (N_2) (nm)	W_0 (CO_2) (cm^3/g)	L_0 (CO_2) (nm)	V_{meso} (cm^3/g)	V_T (cm^3/g)	pH_{pzc}
OTPAC	565	0.24	1.6	0.11	0.66	0.15	0.39	10.7
OSAC	792	0.33	1.2	0.20	0.74	0.06	0.39	10.6
OSAC/KOH	1013	0.43	1.7	0.18	0.73	0.12	0.55	8.3
N	1058	0.44	1.6	0.21	0.88	0.11	0.55	11.6

S_{BET} : BET specific surface area; W_0 : micropore volume; L_0 : mean micropore width; V_{meso} : mesopore volume; V_T : total pore volume ($P/P_0 = 0.95$).

isotherm of OTPAC denotes a more heterogeneous porosity and the predominant mesoporous character. Moreover, microporosity is narrower and homogeneous in the former but larger and heterogeneous in the latter. The CO_2 -adsorption experiments also confirm this heterogeneity, thus, OTPAC present narrower micropores and wider micropores (determined by N_2 -adsorption). In both cases, the presence of the hysteresis cycle in the N_2 adsorption-desorption isotherm confirms the presence of a certain volume of mesopores.

After chemical KOH-activation of OS, the AC obtained (OSAC/KOH) presents a more developed porosity regarding OSAC, with a total pore volume (V_T) of $0.55 \text{ cm}^3/g$ and surface area (S_{BET}) of $1013 \text{ m}^2/g$ (Table 2). Similar properties were obtained under analogous conditions of activation (KOH, $800 \text{ }^\circ\text{C}$, for 2 h) of olive stone-derived char (Stavropoulos and Zabaniotou, 2005). The micropore volume also significantly increased, generating mainly large micropores – W_0 (N_2) –, and so did the corresponding mean micropore width (L_0). Nonetheless, the equivalent narrowest microporosity obtained by CO_2 isotherms – W_0 (CO_2) – didn't alter significantly regarding physical activation. The pore opening also resulted in the generation of mesoporosity, as denoted by the slope of the isotherm, being quite similar to the one obtained for the reference commercial material N.

It is also recognized that the surface chemistry of ACs influences the adsorption process, particularly concerning the presence of oxygen-containing surface groups that may alter the mechanism and extension of the adsorbate-adsorbent interactions (García-Araya et al., 2003). The oxygenated surface groups (OSG) are the main functionalities present on ACs. The surface oxygen content and nature of OSG were analyzed by XPS. The O1s spectral region can be fitted using two components (Fig. 3), assigned to C–O or C=O bonds at ca. 531.8 and 533.4 eV, respectively (Moreno-Castilla et al., 2003). The integrated results are summarized in Table 3. The highest surface oxygen content was observed for OTPAC, which moreover, presents a very homogeneous distribution of OSG containing C=O bonds, like carboxylic acids, but also basic ketones. The OS-derived ACs present smaller oxygen content

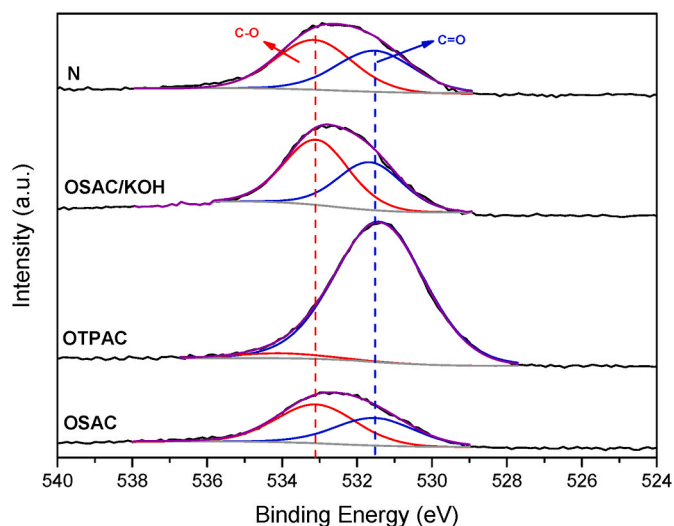


Fig. 3. High resolution XPS spectra of the O1s spectral region for the different biosorbents.

Table 3

Elemental analysis (atomic content, %), species percentages and corresponding binding energies (in brackets, eV) of the different adsorbents determined by XPS analysis.

Sample	O/C	C	O	O1s (%)	
				C=O	C–O
OTPAC	0.11	90.4	9.6	97 (531.4)	3 (534.0)
OSAC	0.06	94.2	5.8	41 (531.5)	59 (533.1)
OSAC/KOH	0.09	92.1	7.9	42 (531.7)	58 (533.1)
N	0.09	91.6	8.4	45 (531.5)	55 (533.2)

than OTPAC, and although this parameter increased after chemical activation, the distribution of C=O and C–O OSG is quite similar in both cases (around 41% and 59%, respectively), denoting the presence of additional groups such as alcohols, phenols, and carboxylic acids. The commercial sample N also presents a high oxygen content, with a very similar distribution of OSG (45% C=O, 55% C–O). The pH at the point of zero charge indicates that all materials present a basic character (Table 2), which was analogous for OSAC and OTPAC samples ($\text{pH}_{\text{pzc}} = 10.6\text{--}10.7$) in spite of their different OSG distribution, and slightly lower in the case of the KOH-activated sample ($\text{pH}_{\text{pzc}} = 8.3$).

3.2. Adsorptive performance of ACs in the treatment of simulated OMW

To evaluate the potential applicability of biosorbents prepared and examine the influence of the OS-activation procedure, the performance of OSAC and OSAC/KOH samples were compared to the commercial AC (N). A simulated OMW was prepared containing 150 mg/L of a mixture of five phenolic compounds, as described in the experimental section. The total phenol removed (Fig. 4) was calculated based on the corresponding concentrations of each product recorded as a function of time along the adsorption experiments (Fig. 5).

The total phenolic content (TPh) uptake decreases in the sense N (257 mg/g) > OSAC/KOH (200 mg/g) > OSAC (189 mg/g). Although sample OSAC/KOH has a very similar porosity as the reference sample N, the TPh removed is approximately 22% lower, which can be related to the lower pH_{pzc} of OSAC/KOH. Chemically activated olive stone presents better performance than the physically activated sample, due to the resulting higher surface area (S_{BET}) and microporosity (W_0) values – Table 2. Nevertheless, while the S_{BET} increases from 792 to 1013 m^2/g (i. e., ca. 28%), TPh removal only improved by 5.8%, which is also indicative that additional parameters should be considered.

The amount of each compound adsorbed also strongly differs between samples (Fig. 5). Only caffeic acid (CA) is quickly and preferentially adsorbed in all samples, with similar q_e values (around 60 mg/g), indicating that it is completely removed in all cases. The commercial sample N also totally adsorbs gallic acid (GA), which is poorly adsorbed on both OS-derived ACs (even on OSAC/KOH that has analogous porosity to sample N). Tyrosol (TY), vanillic (VA), and protocatechuic (PA) acids are only partially removed in all cases, being the amount and

kinetics of adsorption strongly dependent on the adsorbent used.

Experimental data were fitted using well-established kinetic models commonly suited to describe the adsorption process of liquid-solid systems (Wang and Guo, 2020), namely the pseudo-first-order (PFO) (Lagergren, 1898) and pseudo-second-order (PSO) (Blanchard et al., 1984) models. The application of linearized forms of the equations is the most widely used solving method for the determination of both models' parameters, though also entailing the possible introduction of propagation errors by changing the independent/dependent variables (Wang and Guo, 2020). The experimental data was therefore fitted by nonlinear regression, using Microsoft's Excel® solver function with an iterative algorithm that minimizes the residual sum of squares. The results obtained are summarized in Table 4.

For the PFO model, the adsorption is determined by diffusion through a boundary, while PSO is based on the sorption capacity of the solid phase, being commonly assumed that chemisorption could be the rate-controlling step in the adsorption process (Ho and McKay, 1999; Srivastava et al., 2008; Toor and Jin, 2012). The characteristic adsorption constants of PFO and PSO equations were determined according to the integrated rate laws shown in Eqs. (2) and (3), respectively, obtained with the initial condition of $q_t = 0$ at $t = 0$,

$$q_t = q_e (1 - e^{-k_1 t}) \quad (2)$$

$$q_t = \frac{t}{\frac{1}{q_e^2 k_2} + \frac{t}{q_e}} \quad (3)$$

where q_e and q_t are the adsorption capacities (mg/g) at equilibrium and at any given time t (min), respectively, k_1 and k_2 the pseudo-first order (1/min) and pseudo-second order (g/mg min) rate constants. The initial adsorption rate h (mg/g min) can be derived from the PSO model and $dq_t/dt = h$ at $t \rightarrow 0$, according to Eq. (4) (Alhamed, 2009).

$$h = q_e^2 k_2 \quad (4)$$

Both model's applicability/selection was assessed by two statistical indicators: root mean square error (RMSE, Eq. (5)) and correlation coefficient (R^2 , Eq. (6)), being $q_{e,\text{exp}}$ the measured adsorbate concentration in the solid phase and $q_{e,\text{cal}}$ the calculated concentration by any given model (Macedo et al., 2018). Smaller values of RMSE and R^2 values close to the unit indicate minor variations between experimental and calculated data, thus better fittings.

$$\text{RMSE} = \sqrt{\frac{1}{m} \sum_{i=1}^m (q_{e,\text{exp},i} - q_{e,\text{cal},i})^2} \quad (5)$$

$$R^2 = 1 - \frac{\sum_{i=1}^n (q_{e,\text{exp},i} - q_{e,\text{cal},i})^2}{\sum_{i=1}^n (q_{e,\text{exp},i} - \bar{q}_{e,\text{exp}})^2} \quad (6)$$

In all cases, adsorption capacities sharply increase within the first minutes of contact time and the maximum uptake is typically reached after approximately 60 min for the prepared biosorbents, while for commercial sample N it is only reached after 180 min (Fig. 4). Data in Table 4 shows that both models (PFO and PSO) satisfactorily predict the adsorption process for all adsorbents, although the PSO model describes the data slightly better, as suggested by the lower RMSE values when compared to the PFO model. Moreover, PFO doesn't fit well for the entire range of adsorption time, offering the best fittings at the beginning of the process but deviating afterward, thus failing in the theoretical prediction of the amount adsorbed. A similar behavior denoting the deviation of the PFO model was previously described for several adsorbents prepared from agricultural wastes (Salleh et al., 2011).

Globally, the adsorption process appears to be directly linked to the development of the sample's available surface (and therefore porosity) achieved by each activation process; i.e., despite the better fittings obtained using the PSO that suggest that the limiting step is the chemisorption process, the porosity of the samples should be large enough to

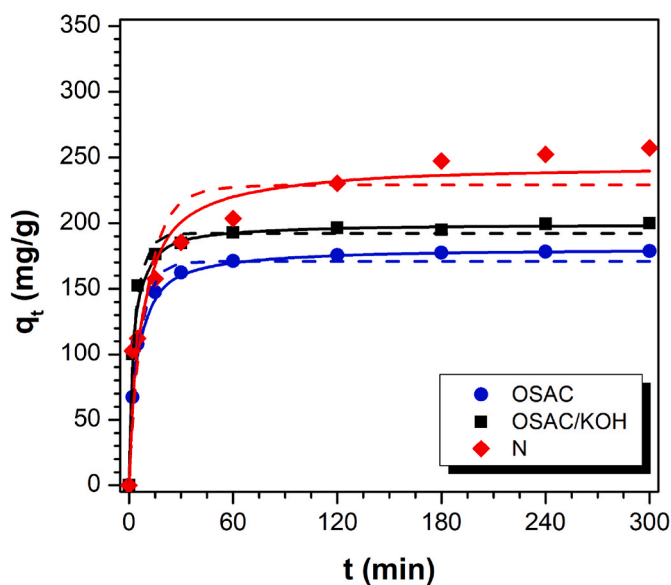


Fig. 4. Total phenol removal as a function of adsorption time (dashed lines: PFO model adjustment; solid lines: PSO model adjustment). Experimental conditions: $C_0 = 150$ mg/L (30 mg/L each phenolic compound) at 25°C , $W_{\text{ads}} = 75$ mg, $\text{pH}_0 = 3.5\text{--}3.8$.

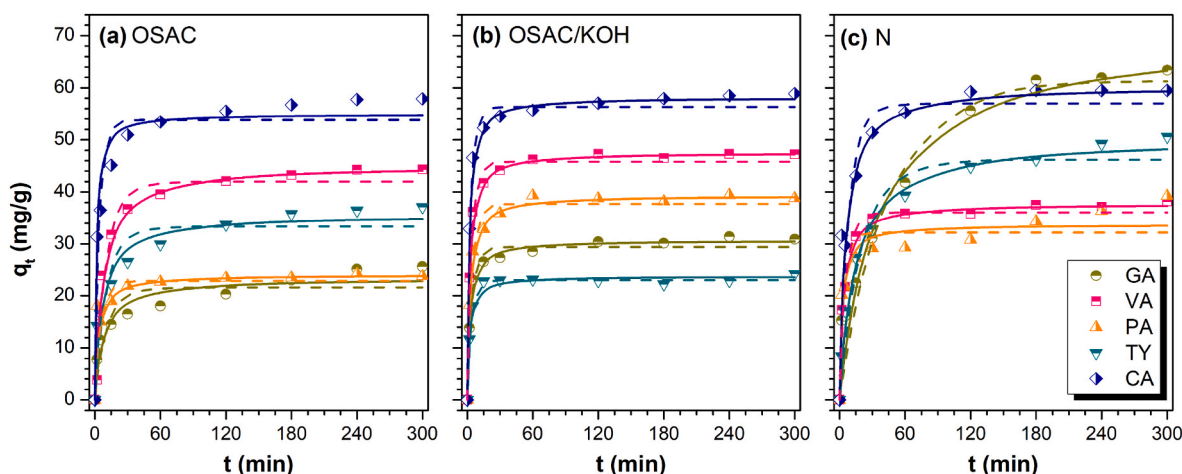


Fig. 5. Kinetic curves for competitive adsorption onto (a) OSAC, (b) OSAC/KOH, and (c) N samples (dashed lines: PFO model; solid lines: PSO model). Experimental conditions: $C_0 = 150$ mg/L (30 mg/L each phenolic compound) at 25 °C, $W_{ads} = 75$ mg, $pH_0 = 3.5$ –3.8.

Table 4

Fitted kinetic parameters of the competitive adsorption runs using the PFO and PSO models.

Adsorbent	Adsorbate	q_e, exp (mg/g)	Pseudo-first order				Pseudo-second order				
			q_e, cal (mg/g)	k_1 (1/min)	RMSE	R^2	q_e, cal (mg/g)	k_2 (g/mg min)	h (mg/g min)	RMSE	R^2
OSAC	GA	25.7	21.6	1.06×10^{-1}	3.2	0.859	23.3	6.19×10^{-3}	3.4	2.2	0.929
	VA	44.4	42.0	1.10×10^{-1}	3.2	0.962	45.0	3.32×10^{-3}	6.7	2.7	0.974
	PA	23.7	22.9	2.25×10^{-1}	1.4	0.970	24.0	1.39×10^{-2}	8.0	0.4	0.997
	TY	37.1	33.4	1.08×10^{-1}	4.2	0.896	35.5	4.66×10^{-3}	5.9	2.7	0.955
	CA	57.9	53.8	3.05×10^{-1}	4.7	0.936	56.2	8.23×10^{-3}	26.0	2.5	0.982
OSAC/KOH	TPh	188.9	170.8	2.12×10^{-1}	17.8	0.915	180.7	1.64×10^{-3}	53.5	10.2	0.972
	GA	30.9	29.4	3.07×10^{-1}	1.5	0.979	30.7	1.51×10^{-2}	14.2	0.9	0.991
	VA	47.2	45.8	3.33×10^{-1}	1.7	0.988	47.5	1.12×10^{-2}	25.3	0.8	0.998
	PA	38.8	37.7	2.98×10^{-1}	1.9	0.978	39.3	1.16×10^{-2}	17.9	0.9	0.995
	TY	24.3	23.0	3.31×10^{-1}	0.6	0.995	23.7	2.41×10^{-2}	13.6	0.9	0.987
N	CA	58.9	56.3	4.02×10^{-1}	2.1	0.986	58.1	1.18×10^{-2}	39.8	0.9	0.998
	TPh	200.0	192.2	3.40×10^{-1}	7.2	0.988	199.3	2.75×10^{-3}	109.1	3.0	0.998
	GA	63.4	61.3	2.42×10^{-2}	4.4	0.979	70.1	4.40×10^{-4}	2.2	3.3	0.986
	VA	38.2	36.1	2.20×10^{-1}	2.2	0.970	37.7	9.11×10^{-3}	12.9	1.1	0.993
	PA	39.2	32.2	3.33×10^{-1}	4.1	0.865	33.7	1.43×10^{-2}	16.2	3.1	0.922
	TY	50.6	46.2	5.52×10^{-2}	3.8	0.963	50.2	1.58×10^{-3}	4.0	1.8	0.990
	CA	59.5	57.0	1.39×10^{-1}	4.2	0.963	60.3	3.47×10^{-3}	12.6	1.7	0.993
	TPh	257.1	229.0	1.17×10^{-1}	29.5	0.889	244.1	7.18×10^{-4}	42.8	19.2	0.950

avoid several diffusion restrictions. This was in agreement with the larger micropore volumes detected with N_2 at -196 °C regarding those observed with CO_2 at 0 °C, confirming the absence of diffusional problems of N_2 at low temperatures into the micropores.

The simulated OMW presents an acidic character ($pH = 3.8$) as a result of the dissociation of the four phenolic acids (pK_a values ≈ 4), whereas anionic-neutral species are expected in the case of TY ($pK_a = 10.2$). Under such conditions, all carbon surfaces should be positively charged due to their demarked basic character ($pH_{pzc} = 8.3$ –11.6). Generally speaking, attractive interactions between adsorbents and adsorbates should favor the adsorption of deprotonated compounds, in agreement with the better fittings observed with the PSO model. Nevertheless, repulsive interactions are observed between TY and the AC surfaces, both positively charged at the solution's pH. In fact, tyrosol is the less adsorbed compound on OSAC/KOH (Fig. 5).

Moreover, despite the similar porosity and pore size distribution between OSAC/KOH and N samples, the adsorption capacity of the former is generally smaller in comparison, whereas the initial adsorption rate (h , Table 4) is always higher. Likewise, despite the complete CA adsorption observed in all cases, it occurs faster than the remaining compounds in solution on either OSAC or OSAC/KOH, whereas h values obtained for CA onto commercial sample N are comparable to those of

VA or PA (which were, ultimately, the less adsorbed compounds in this case). The overall worse fittings (higher RMSE values) obtained for sample N also denotes the greater heterogeneity of this sample.

Competitive adsorption processes are complex and determined not only by the combination of porosity and surface area of the adsorbent (determining accessibility and extent of the active surface) and the interaction with the adsorbates (nature and concentration of functional groups) but also by interactions occurring between the different adsorbates in solution. In general, the presence of various adsorbates in solution leads to inhibitory effects and a worse elimination of pollutants (Li et al., 2019). Considering these results, GA and VA were selected to perform individual adsorption experiments to further elucidate the physicochemical properties controlling such adsorbent-adsorbate interactions.

3.3. Performance of ACs in the adsorption of single phenolic compounds

Adsorption models allow us to infer the adsorption mechanism occurring in such solid-liquid/gas systems and to determine specific equilibrium parameters, key to the design and development of adsorption processes (Jeguirim et al., 2018; Ayawei et al., 2017). To better describe and quantify the equilibrium relationship between each solute

and the adsorbents tested, several isotherms were fitted to the experimental data, including Langmuir, Freundlich, Sips, Langmuir-Freundlich, and Radke-Prausnitz (Wanassi et al., 2017). To check the models' adhesion, a mathematical/model selection criterion (MSC) was applied in addition to R^2 and RMSE. As detailed elsewhere (Macedo et al., 2018), MSC takes also into account the number of fitting parameters of the model and the number of experimental points. For brevity, the results presented here are those where better models adhesion to experimental data was achieved: with the Langmuir and Freundlich isotherms.

The Langmuir isotherm is based on the hypothesis that adsorbate molecules form a uniform and finite monolayer on the adsorbent's surface (Seader et al., 2010). The nonlinear form of the Langmuir model can be represented according to Eq. (7),

$$q_e = \frac{q_m K_L C_e}{1 + K_L C_e} \quad (7)$$

where C_e is the equilibrium solute concentration (mg/L), q_m is the maximum uptake of adsorbed molecules per unit mass of adsorbent (mg/g) for the formation of a complete monolayer on the adsorbent's surface, q_e the equilibrium concentration in the adsorbent phase (mg/g), and K_L the adsorption constant of the Langmuir isotherm equation (L/mg). The product $K_L q_m$ is often used to describe the relative affinity of the adsorption process (Rivera-Utrilla et al., 1993).

The Freundlich isotherm is commonly apt to describe non-ideal sorption on highly heterogeneous surfaces that provide adsorption sites of varying affinities (Seader et al., 2010). The model's nonlinear form can be represented as described in Eq. (8),

$$q_e = K_F C_e^n \quad (8)$$

where K_F the Freundlich constant related to adsorption capacity ((mg/g) (mg/L)ⁿ), and n an empirical parameter related to the adsorption intensity.

Overall, both models describe the experimental adsorption data reasonably well (fittings shown in Fig. 6). Based on the calculated statistical parameters (Table 5), the overall uptake process of gallic acid approaches the Freundlich model better (higher R^2 and lower RMSE values) than the Langmuir one, whereas the latter seems to better describe the adsorption of vanillic acid (except for N). Moreover, the Langmuir isotherm typically predicted more accurately the behavior at lower concentrations of sorbate in equilibrium (formation of a monolayer), while at higher concentrations the Freundlich model was better apt to describe the process of multilayer adsorption in some cases (cf. Fig. 6). The highest values of the RMSE parameter were always obtained

for the commercial activated carbon N, which is the only material that obeys the Freundlich isotherm for both GA and VA, thus suggesting a multilayer adsorptive behavior independently of the adsorbate.

As in the case of the TPh analysis provided in Section 3.2 for the competitive process, the adsorption isotherms of both GA and VA reflect the smaller adsorption capacity of OTPAC for the range of materials studied, and that commercial sample N always offers the best results. Comparing the influence of the raw bio-residue material on physically activated samples, GA is preferentially adsorbed regarding VA in the case of OTPAC, while the contrary performance is observed for OSAC. Nevertheless, the chemically activated OSAC/KOH has a similar GA or VA adsorption capacity, and this performance is also observed for the reference N-sample. The values of both constants (K_L and K_F) were always higher for the uptake of gallic acid than the corresponding ones for vanillic acid. Thus, the product $K_L q_m$, related with the affinity of the adsorption processes, is almost always higher for GA than for VA, independently of the adsorbent used, and increases upon increasing the microporosity and surface area of the materials. Thus, adsorbents derived from the olive stone precursor showed higher maximum monolayer adsorption capacities (q_m) than the one prepared from olive tree pruning. Likewise, chemical activation also favors microporosity and consequently the uptake capacity (Table 5).

Despite the lower capacity obtained for the OTPAC sample, the morphological and porous characteristics of this sample, including the well-developed network of wider channels, may favor de adsorption (removal/recovery) of larger molecules, or its use for the development of micro/mesoporous metal supports for heterogeneous catalysts.

Adsorption kinetics were also investigated based on the uptake of gallic and vanillic acids at 25 °C. Fig. 7 compares the PFO and PSO models prediction for each adsorbent (dashed and solid lines, respectively) with the experimental values (dots) for the two phenolic compounds.

There is a good agreement between the experimental adsorption capacity values and those predicted by the models. As postulated in the previous section, the experimental adsorption capacities obtained in this series of experiments (q_e values, Table 6) are, in general, higher than those obtained for the same experimental conditions (same C_0 as the ones here reported) when various adsorbates compete for adsorption sites (cf. TPh values in Table 4). All PSO kinetic parameters values progressively increased in the sense OTPAC < OSAC < OSAC/KOH. However, in spite of the higher q_e values obtained for sample N, smaller k_2 and h values are obtained regarding OSAC/KOH, as well as in general, worse fittings.

When using physically activated olive stone-derived sample (OSAC), the experimental equilibrium adsorption capacity for TPh removal in the

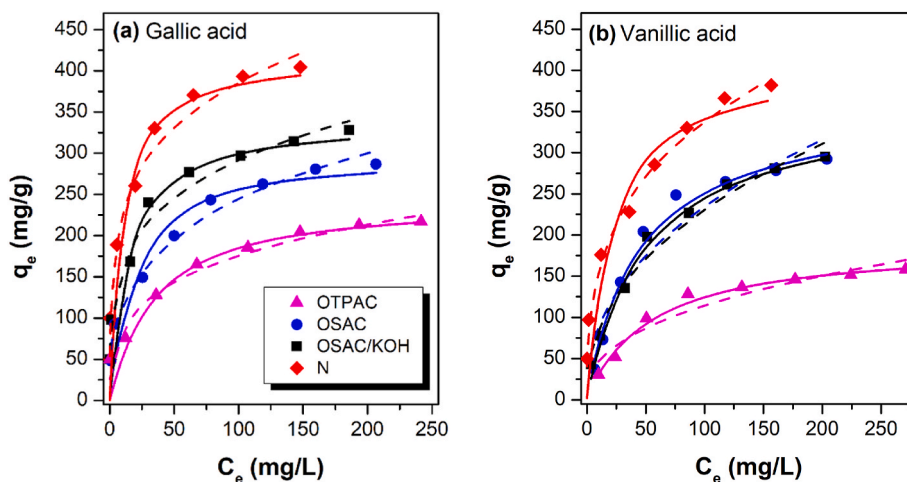


Fig. 6. Adsorption isotherms of (a) gallic acid and (b) vanillic acid (solid lines: experimental data fit with Langmuir isotherm; dashed lines: fit with Freundlich isotherm). Experimental conditions: 25 °C, $C_0 = 25$ –350 mg/L, $W_{ads} = 25$ mg, $V = 50$ mL, $pH_0 = 3.5$ –3.8.

Table 5
Langmuir and Freundlich isotherm models' parameters for gallic and vanillic acids.

Adsorbate	Adsorbent	Langmuir				Freundlich			
		q_m (mg/g)	K_L (L/mg)	RMSE	R^2	n	K_F ((mg/g)/(mg/L) ⁿ)	RMSE	R^2
Gallic Acid	OTPAC	244.0	0.032	18.0	0.972	0.27	50.1	16.0	0.943
	OSAC	296.0	0.067	19.6	0.970	0.29	65.7	10.7	0.984
	OSAC/KOH	337.6	0.082	32.1	0.966	0.24	98.5	12.7	0.983
	N	416.6	0.120	40.6	0.971	0.21	144.4	14.8	0.987
Vanillic Acid	OTPAC	188.6	0.020	5.0	0.988	0.39	19.3	12.4	0.927
	OSAC	359.0	0.024	10.3	0.989	0.42	34.2	26.4	0.920
	OSAC/KOH	358.5	0.022	9.2	0.992	0.42	33.0	13.5	0.978
	N	406.9	0.053	34.7	0.960	0.31	82.4	9.3	0.994

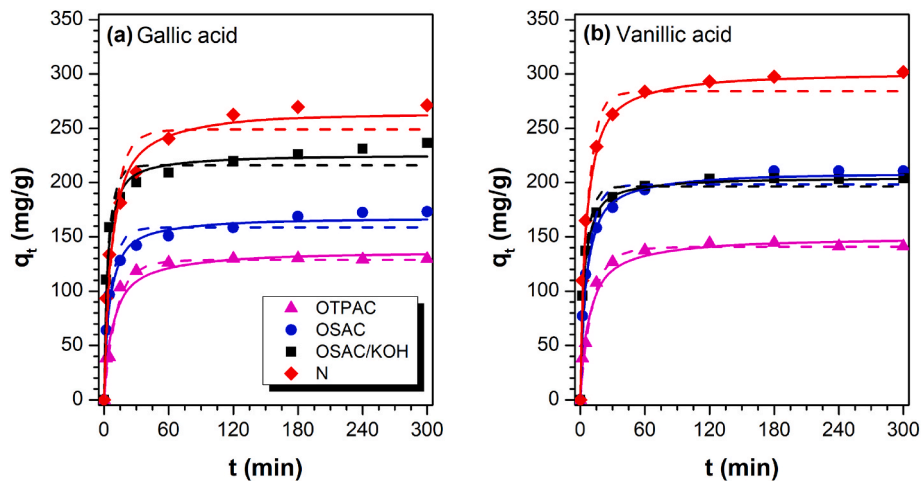


Fig. 7. Kinetic curves for (a) gallic acid and (b) vanillic acid adsorption at $C_0 = 150$ mg/L, 25°C , $V = 50$ mL, $\text{pH}_0 = 3.5\text{--}3.8$ (dashed lines: fitting of PFO model to experimental data; solid lines: fitting of PSO model).

Table 6
Fitted parameters for the pseudo-first order and pseudo-second order kinetic models.

Adsorbate	Adsorbent	Pseudo-first order					Pseudo-second order				
		$q_{e, exp}$ (mg/g)	$q_{e, cal.}$ (mg/g)	k_1 (1/min)	RMSE	R^2	$q_{e, cal.}$ (mg/g)	k_2 (g/mg min)	h (mg/g min)	RMSE	R^2
Gallic Acid	OTPAC	129.8	128.6	1.02×10^{-1}	5.7	0.987	136.6	1.12×10^{-3}	20.8	6.6	0.982
	OSAC	173.3	158.7	1.87×10^{-1}	12.8	0.956	168.1	1.55×10^{-3}	43.8	5.9	0.989
	OSAC/KOH	236.4	215.8	3.00×10^{-1}	15.0	0.966	225.7	1.96×10^{-3}	100.0	7.5	0.989
	N	271.1	248.9	1.33×10^{-1}	24.7	0.936	267.4	7.04×10^{-4}	50.3	12.3	0.983
Vanillic Acid	OTPAC	141.3	140.7	9.90×10^{-2}	5.4	0.991	149.7	9.86×10^{-4}	22.1	5.2	0.990
	OSAC	210.6	198.2	1.70×10^{-1}	14.5	0.962	209.9	1.16×10^{-3}	51.2	5.2	0.995
	OSAC/KOH	203.9	196.2	2.70×10^{-1}	10.5	0.977	204.9	2.02×10^{-3}	84.6	2.2	0.999
	N	301.8	284.1	1.74×10^{-1}	17.8	0.973	302.1	8.30×10^{-4}	75.8	4.3	0.998

competitive adsorption run is 189 mg/g (Table 4), an intermediate value regarding the GA (173 mg/g) and VA (211 mg/g) removals when this biosorbent was applied in the single adsorption process (Table 6). Regarding the kinetic constant k_2 , the computed value is 1.64×10^{-3} in the competitive run, which is also comparable to the k_2 values for single GA (1.55×10^{-3}) or VA (1.16×10^{-3}) adsorption processes. It is worth noting that, for the same conditions of C_0 , the apparent reaction rate constants were always in the same order of magnitude, except for commercial sample N (with k_2 values one order of magnitude lower).

Similarly, for the chemically activated sample (OSAC/KOH), TPh is 200 mg/g (Table 4), also comparable to 204 mg/g of VA or the 236 mg/g of GA (Table 6). However, using the commercial sample N, $q_{e,exp}$ values for TPh in competitive adsorption experiments is 257 mg/g, thus significantly smaller than the 302 mg/g of VA or 271 mg/g of GA removed from single adsorption experiments. Thus, a greater inhibitory effect is observed for commercial N sample than in our biosorbents,

which could favor their application for the treatment of real OMW.

The mass transfer process of gallic and vanillic acids was analyzed using a known intraparticle diffusion model, based on the theory proposed by Weber and Morris (1963), according to Eq. (9),

$$q_t = K_{id} t^{1/2} + C \quad (9)$$

where K_{id} is defined as the intraparticle diffusion rate constant (mg/g $\text{min}^{1/2}$), and C (mg/g) is a constant related to the boundary layer thickness, i.e. larger values of C suggest a greater boundary layer effect (Fierro et al., 2008). The plot of q_t vs. $t^{1/2}$ (Fig. 8) shows that a linear behavior is not obtained for the entire time range, indicating that different steps influence the adsorption processes (Pholosi et al., 2020). Results of the fittings of each linear section are collected in Table 7. From a mechanistic point-of-view, the adsorption process may be controlled by one or more steps, including: i) solute diffusion from the bulk solution to the adsorbent's external surface; ii) mass transfer within

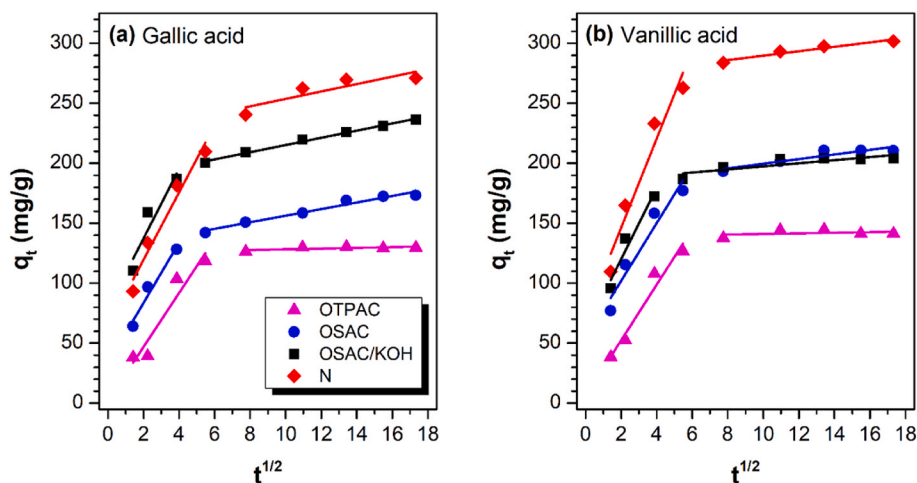


Fig. 8. Intraparticle diffusion adsorption kinetics for (a) gallic acid and (b) vanillic acid at $C_0 = 150$ mg/L, 25 °C, $V = 50$ mL, and $pH_0 = 3.5$ – 3.8 .

Table 7

Intraparticle diffusion parameters for the adsorption of gallic and vanillic acids.

Adsorbate	Adsorbent	1st linear part of the curve			2nd linear part of the curve		
		$K_{id,1}$ ($\text{mg/g min}^{1/2}$)	C_1 (mg/g)	R^2	$K_{id,2}$ ($\text{mg/g min}^{1/2}$)	C_2 (mg/g)	R^2
Gallic acid	OTPAC	21.8	4.8	0.944	0.4	123.9	0.912
	OSAC	25.1	33.3	0.961	2.7	128.9	0.969
	OSAC/KOH	29.0	79.4	0.884	3.0	185.2	0.993
	N	28.0	63.5	0.962	5.0	195.9	0.802
Vanillic acid	OTPAC	23.2	6.1	0.961	0.2	142.5	0.936
	OSAC	32.0	36.7	0.975	2.8	168.3	0.868
	OSAC/KOH	29.8	60.4	0.947	1.3	184.5	0.722
	N	37.1	71.9	0.946	1.8	271.3	0.946

the particle (pore diffusion); iii) solute's uptake onto adsorption-sites, which can involve different mechanisms (e.g. adsorption, ion-exchange, complexation, chelation) (Toor and Jin, 2012; Viegas et al., 2014; Conde et al., 2017).

The two straight lines in Fig. 8 indicate that the GA or VA intraparticle transport to the carbon surface occurs in two steps with very different adsorption rates (slope, K_{id}). The first one corresponds to diffusion into the open porosity (macro-meso-large micropores) and the second one, slower, corresponds to diffusion into narrow micropores (Conde et al., 2017; Allen et al., 1989). The smallest C values are observed for OTPAC, suggesting a smaller boundary layer effect for both GA and VA adsorption onto this sample, which is a direct consequence of the predominant open porosity (large channels observed by SEM, Fig. 1). The boundary layer effect increased in the same order: OTPAC < OSAC < OSAC/KOH. The highest C values are always observed for the most porous samples, OSAC/KOH and N, due to the fundamental microporous character of these samples, in spite of the significant mesopore volume observed (Table 2). After that, phenolic molecules diffuse into the microporosity (Toor and Jin, 2012; Mohd Din et al., 2009), first occupying large micropores (typically determined by N_2 -adsorption), and in a second step to the ultramicropores (narrower than 0.7 nm, determined by CO_2 -adsorption). The intraparticle diffusion rate constant K_{id} values increased with increasing the microporous volume (surface) accessible to the adsorbate and are typically greater for VA than GA. It is also noteworthy that $K_{id,1} \gg K_{id,2}$ because ultramicropores present a size that approaches the phenolic molecules' size (Table 1), which strongly limits their diffusion inside this microporosity range (Toor and Jin, 2012;

Conde et al., 2017; Mohd Din et al., 2009). A plateau is even approached in the case of OTPAC, indicating a very low adsorption rate/capacity in the second stage, which seems to be related to the least developed and narrower ultra-microporosity observed in this sample (Table 2).

Thus, the adsorptive performance of the samples in this series, including adsorption capacity or mass transfer process, is mainly determined by the differences in the pore structure. A relation between adsorption capacities and textural properties (S_{BET} and W_0 (N_2)) can therefore be established, as shown in Fig. 9. The highest adsorption capacities were achieved with the AC with better developed large micropores (sample N), whereas the pruning waste-derived adsorbent OTPAC exhibited the lowest adsorption capacity towards both contaminants. However, narrow ultramicropores have a very low influence on the adsorption capacity or adsorption rate (Table 7). Similarly, in spite of the predominant mesoporous character of the OTPAC sample that leads to the smaller restriction in the external film diffusion, the initial adsorption rate h for GA and VA calculated from the PSO model (Table 6) is also the lowest (20.8 and 22.1 mg/g min, whereas h values ranging from 43.8 to 100.0 mg/g min are observed for the remaining ACs). Thus, the extent of S_{BET} , more than the microporous surface, seems

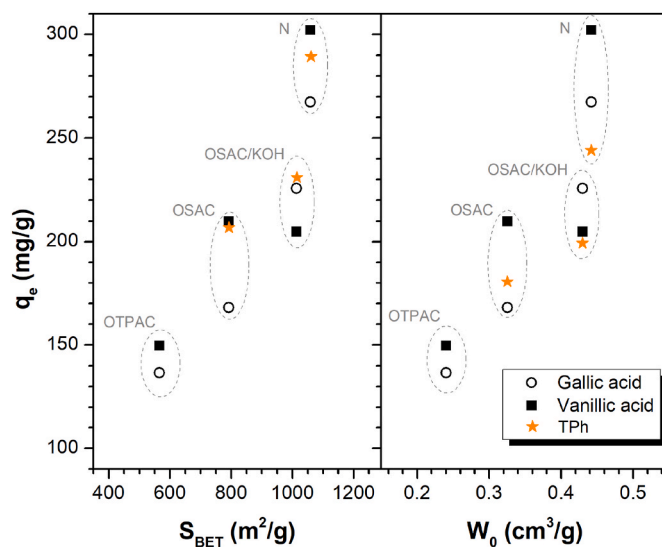


Fig. 9. Relationship between equilibrium adsorption capacities (q_e) and the textural characteristics (S_{BET} and W_0 (N_2)) of the adsorbents for gallic and vanillic acids ($C_0 = 150$ mg/L); q_e values for TPh on competitive runs shown for comparison (same experimental conditions).

Table 8

Comparison of maximum adsorptive capacities (mg/g) of various low-cost adsorbents derived from agro-industrial residues for different organic pollutants (at 25 °C).

Adsorbent	Adsorbate	q _m (mg/g)	Ref.
OS and OTP derived-ACs	Phenolic compounds	188.6–359.0	This work
Partially-combusted OP	Total phenol from OMW	11.4	Stasinakis et al., (2008)
OS-derived AC	Dye (Methylene blue)	16.1	Hazzaa and Hussein, (2015)
Olive-waste cake derived AC	Dye (Lanaset grey G)	108.7	Baccar et al., (2010)
Solvent-washed OWs	Phenol, nitrophenols, chlorophenols	5.5–12.3	El-Sheikh et al., (2013)
OH-derived ACs	Phenolic compounds	58.3–284.6	Michailof et al., (2008)
OS-derived AC	Total phenol/COD from OMW	91.7/1667	Galiatsatou et al., (2002)
Solvent-extracted olive pulp AC		71.4/1429	
OS- derived AC	Hydroxytyrosol	375.0	Eder et al., (2021)
OH-derived MgCl ₂ -AC	Phenol, PMP, PNP	43.9–122.0	Hamadneh et al., (2020)
OS-derived KOH-ACs	Dye (Methylene blue)	190–263	Stavropoulos and Zabaniotou, (2005)

OS – Olive stone; OTP – Olive tree pruning; OP – Olive pomace; OW – Olive wood; OH – Olive husk.

to be the main parameter governing the adsorption of phenolic compounds, mesopores, and large micropores W_0 (N_2) are determining the adsorption rate and uptake of the adsorbate molecules (Fig. 9). In general, adsorption capacities determined at equilibrium by the PSO model were globally higher in the case of vanillic acid (Table 6). However, from the analysis of the GA or VA isotherms (Table 5) it is observed that affinity presents the contrary trend, namely pointed out by the higher values of K_L and K_F for GA.

Nevertheless, additional parameters, associated to the characteristics of the phenolic compounds should also be taken into account. The influence of interactions adsorbent-adsorbate was pointed out by the best fittings reached with the PSO model. In previous works, it was demonstrated that carbon materials' adsorption of phenols is influenced by parameters such as their solubility in water (the higher solubility the smaller adsorbability, i.e. greater affinity by water) (Michailof et al., 2008; García-Araya et al., 2003; Kumar et al., 2003). Nonetheless, results in this study show that caffeic and vanillic acids, with similar solubility and pKa (Table 1), exhibited very distinct adsorption behaviors. Similarly, the higher solubility of TY regarding the rest of phenolic acids should induce a smaller adsorption, however, an intermediate adsorption behavior is observed in many cases. The affinity of different phenols by the carbon surface also varies according to the nature of the aromatic rings substituents (Moreno-Castilla et al., 1995). Adsorption of phenols is favored by the withdrawing effect of substituents, which modify the electron density of the aromatic rings and consequently the strength of the π - π interactions with the carbon surface. In a previous work by Michailof et al. (2008), the following order of deactivation of the aromatic ring was established: vanillic acid > caffeic acid > gallic acid, though caffeic acid was also the best-adsorbed compound in spite of the degree of deactivation of the aromatic ring (in line with the results obtained in our study). The shape and molecular dimensions of phenols can also determine the accessibility and interactions with the adsorbent surface. The molecular shape of CA is almost linear with a length of 8.7 Å, while the maximum linear dimension of VA and GA is similar and approximately 6.4 Å. Thus, the micropore size determined from the N_2 -adsorption isotherms is, in all cases, clearly larger than the molecular dimension of the adsorbates.

Regarding the chemical characteristics of the carbon surface, oxygenated surface groups are the main functionalities, and it was demonstrated that by increasing the oxidation degree, phenols' adsorption is progressively reduced (Sun et al., 2019). Fierro et al. (2008) described the beneficial effect of basic sites and carbonyl groups located in larger micropores leading to donor-acceptor interactions, in competition with the π - π interactions mainly developed inside the narrowest micropores. In our case, the oxygen content increases with the chemical activation, but this process is accompanied by a development of the porosity, similarly, the larger amount of C=O found in OTPAC can be countered by the smaller microporosity of this sample, thus the variation in the oxygen content of these biosorbents do not provide clear information. Table 8 shows a summary of the maximum adsorptive

capacities of similar adsorbents (i.e., prepared from olive mill's agro-industrial by-products) reported in the scientific literature for various adsorbates. Despite of the different raw materials and activation processes used and activation degrees reached, it is noteworthy that in general, our adsorbents present a better performance than those typically described. For instance, Eder et al. (2021) prepared olive pit derived-AC by physical activation with water vapor and reported on the application of the resulting material for hydroxytyrosol removal. The resulting adsorbent presented considerably high specific surface area ($S_{BET} = 1040 \text{ m}^2/\text{g}$), total pore volume ($0.69 \text{ cm}^3/\text{g}$), and average pore size (4.4 nm), and the maximum adsorption capacity achieved was 375 mg/g. These values are of the same order as those obtained in our case by one-step chemical activation of OS with KOH. Hamadneh et al. (2020) selected olive husk for the synthesis of AC using MgCl_2 as activating agent. The biosorbent presented BET surface area, total pore volume, and average pore size of $484 \text{ m}^2/\text{g}$, $0.07 \text{ cm}^3/\text{g}$, and 1.5 nm, respectively. The maximum adsorbent capacities reported for phenol, p-methoxyphenol, and p-nitrophenol were 43.9, 98.0, and 122.0 mg/g, respectively, and the process was well described by the Langmuir isotherm model in all cases. Thus, the selection of the raw materials and the adequate activation procedure is the key factor to obtain optimized biosorbents.

The results obtained with our biosorbents also clearly improve those presented in studies using commercial neutral or ionic exchange resins for the recovery of phenols from OMW, which showed a maximum adsorption capacity of 81 mg/g (Frasconi et al., 2019). Nevertheless, macroreticular polymers displayed poor adsorption capacity, but allow a high selectivity for the separation of some compounds from OMW, such as hydroxytyrosol (Yanguí et al., 2017). Other advanced carbon materials, like graphene oxide foams with hierarchical interconnected porous texture (Wang et al., 2019) showed a maximum phenol adsorption capacity of 135.6 mg/g, although increased for different chlorobenzenes.

In sum, the development of the porous structure is a key parameter to improve the adsorptive capacity, but the synthesis procedure should also be modeled/tuned to consider the functionalization of the adsorbents to target specific compounds within a complex matrix (such is the case of some phenolic compounds, often suitable for applications related to their antioxidant properties in different industries), which should be subsequently recovered through and optimized desorption process, aiming to isolate and concentrate them (e.g., tyrosol and hydroxytyrosol).

3.4. Regeneration of adsorbents

For practical applications, the stability and reusability of the adsorbents are of utmost importance. After adsorption capacities were evaluated for the uptakes of GA or VA, spent samples were thermally regenerated in N_2 flow, and the regenerated samples were used again in the same experimental conditions. To determine if thermal regeneration

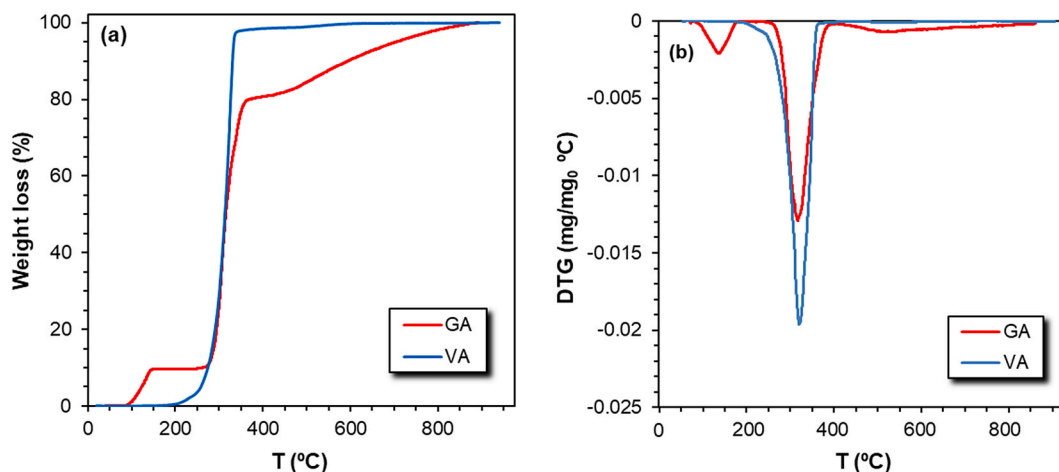


Fig. 10. (a) TG and (b) DTG profiles of gallic acid (GA) and vanillic acid (VA) decomposition.

is an appropriate technique (and the required experimental conditions), the thermal behavior of GA and VA acids were tested by TG/DTG experiments (Fig. 10). For VA, single-step and complete decomposition take place at around 330 °C, while the decomposition of GA presents an initial small weight loss (WL) at low temperature and then total decomposition occurs slower in comparison to VA and up to higher temperatures.

Fig. 11 compares TG/DTG curves of fresh and spent OSAC/KOH samples. The WL of the fresh sample is associated with desorption of adsorbed compounds, namely water, and the removal of oxygenated surface groups of different thermal stability that evolve as CO and CO₂. Carboxylic acid groups present in the adsorbent are typically desorbed as CO₂ at low temperature (<400 °C), while CO-desorption in this range corresponds to carbonyl groups in α -substituted ketones and aldehydes. Anhydride groups decompose evolving a mixture of CO + CO₂ at around 550 °C, and lactones as CO₂ at 650 °C. Finally, the more stable and basic surface groups evolve as CO at high temperature, phenolic and hydroquinone groups at around 720 °C, and carbonyl or quinones above 900 °C (Morales-Torres et al., 2010b).

TG profiles of fresh and spent samples are coincident with increasing temperature up to around 330 °C, i.e., the temperature range where the decomposition of GA and VA occurs. However, the DTG of spent samples does not show a sharp peak at 330 °C corresponding to the decomposition of adsorbed GA or VA observed for pure adsorbates (Fig. 10). When fixed on the adsorbent surface, their decomposition takes place progressively with increasing temperature. From 600 °C on, the WL

observed is also enhanced by the release of OSG present in the fresh sample. According to data in Table 5, spent samples contain 337 mg/g of GA and 358 mg/g of VA, i.e., between 34 and 36% of the total weight, corresponding approximately to the difference observed in the TG profiles of fresh and spent samples at 800 °C.

Thus, regeneration of spent samples was carried out in 40 min, by heating at a rate of 20 °C/min up to 800 °C without soak time. After cooling, regenerated samples were used again in identical adsorption experimental conditions, and results are summarized in Fig. 12. Comparing the results obtained with those of Fig. 7 and Table 6, it is clear that adsorption capacities after 300 min decreased by different degrees depending on the adsorbent. Both textural and chemical transformations associated with the formation of permanent deposits, or on the contrary, gasification processes of the supports, will be responsible for this adsorption capacity decrease. Although significant deactivation was observed for OSAC/KOH and N (i.e., the best microporous adsorbents), OSAC shows a minor adsorption capacity decrease of approximately 8–12%, depending on the adsorbate. This means that the thermal cycle for the regeneration process should be optimized according to the biosorbents characteristics, although heating in an inert atmosphere is an efficient, cheap, and fast regeneration procedure.

4. Conclusions

A series of biosorbents (ACs) was prepared by physical or chemical activation of residues from the olive oil production (olive stone, OS, and

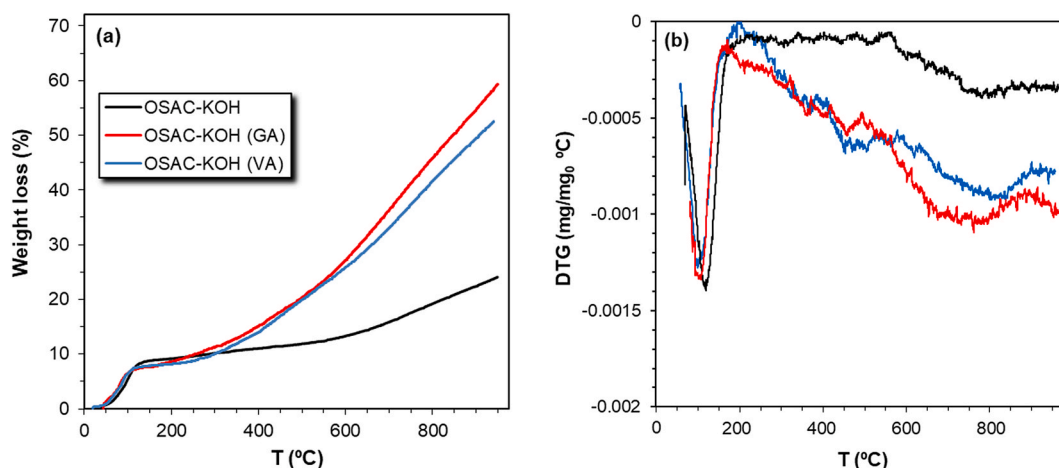


Fig. 11. (a) TG and (b) DTG profiles of fresh and spent OSAC/KOH after adsorption of GA or VA.

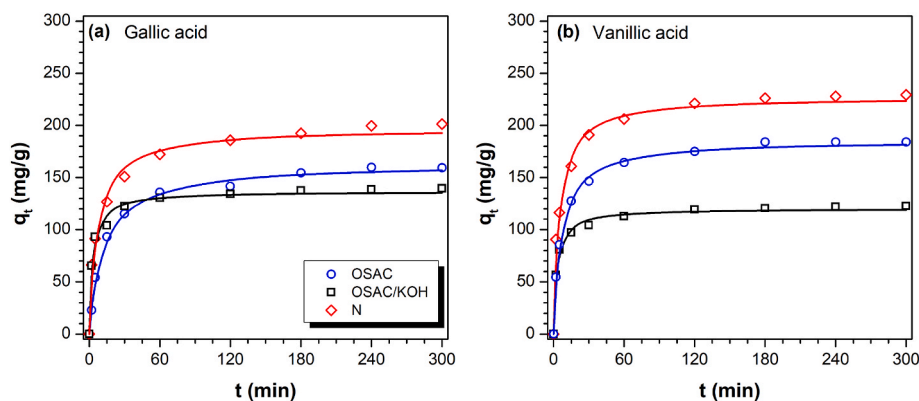


Fig. 12. Kinetic curves for (a) gallic and (b) vanillic acids using regenerated samples at $C_0 = 150$ mg/L and 25 °C (PSO model adjustment).

rest of pruning, OTP). The resulting porosity and chemical nature depend on the raw materials, OTPAC showing a more open structure and homogeneous oxygenated surface groups but smaller microporosity and surface area. Chemical activation of OS with KOH produces, in only one synthesis step, greater development of porosity, namely the microporosity. The total pore volume of the materials tested ranged from 0.39 to 0.55 cm^3/g and S_{BET} from 565 to 1013 m^2/g .

The competitive adsorptive performance in simulated OMW was compared with the adsorption of single phenolic compounds (vanillic and gallic acids, VA and GA). Adsorption kinetics were fitted using PFO and PSO models, as well as the intraparticle diffusion model. The adsorption isotherms of VA and GA were fitted by applying the Langmuir and Freundlich equations. The best fittings were obtained using the PSO model, suggesting the influence of chemical interactions in the global process. The transport of the phenolic compounds to the carbon surface occurs in two steps, corresponding to the process inside large pores and narrow micropores, respectively, with the latter showing a scarce influence in the global adsorptive process. Thus, the adsorption capacity and adsorption rate are mainly determined by the porosity, specifically by the larger micropores and the BET surface area, rather than the samples' total micropore volume.

High total phenolic content (TPH) adsorption capacities (q_e) were observed along the competitive adsorption process with simulated OMW, also comparable to those obtained in single VA or GA adsorption processes, while a commercial AC from Norit, used as a reference, shows a significant inhibition degree in the competitive adsorption runs. Regeneration by thermal treatment demonstrated high efficiency for OSAC, allowing the reuse of this adsorbent, though the process should be further optimized for the entire range of materials studied. These results evidenced the applicability of such biosorbents in the removal of OMW phenolic compounds.

Author contributions

Conceptualization, F.J.M.-H., and L.M.M.; investigation, B.M.E. and S.M.-T.; writing—original draft preparation, B.M.E.; writing—review and editing, S.M.-T., F.J.M.-H., and L.M.M.; supervision, F.J.M.-H., and L.M.M.; funding acquisition, L.M.M., F.J.M.-H., and S.M.-T. All authors have read and agreed to the published version of the manuscript.

Declaration of competing interest

The authors declare that they have no known competing financial interests or personal relationships that could have appeared to influence the work reported in this paper.

Acknowledgments

This work was financially supported by: Base funding - UIDB/00511/

2020 of the Laboratory for Process Engineering, Environment, Biotechnology and Energy - LEPABE – funded by national funds through the FCT/MCTES (PIDDAC); Project NORTE-01-0247-FEDER-39789 funded by European Regional Development Funds (ERDF) through North Portugal Regional Operational Programme (NORTE 2020); Project “HealthyWaters – Identification, Elimination, Social Awareness and Education of Water Chemical and Biological Micropollutants with Health and Environmental Implications”, with reference NORTE-01-0145-FEDER-000069, supported by NORTE 2020, under the PORTUGAL 2020 Partnership Agreement, and through the Spanish Project ref. RTI2018-099224-B-I00 from MCIN/AEI/10.13039/501100011033/FEDER “Una manera de hacer Europa”. Bruno Esteves is grateful to FCT for financial support through the PhD grant (SFRH/BD/129235/2017), with financing from National and the European Social Funds through the Human Capital Operational Programme (POCH). Sergio Morales-Torres acknowledges the MCIN/AEI/10.13039/501100011033 and the European Social Found (FSE) “El FSE invierte en tu futuro” for a Ramón y Cajal research contract (RYC-2019-026634I). Authors acknowledge the funding for open access charge: Universidad de Granada / CBUA.

References

- Aggoun, M., Arhab, R., Cornu, A., Portelli, J., Barkat, M., Graulet, B., 2016. Olive mill wastewater microconstituents composition according to olive variety and extraction process. *Food Chem.* 209, 72–80. <https://doi.org/10.1016/j.foodchem.2016.04.034>.
- Ahmaruzzaman, M., 2008. Adsorption of phenolic compounds on low-cost adsorbents: a review. *Adv. Colloid Interface Sci.* 143, 48–67. <https://doi.org/10.1016/j.cis.2008.07.002>.
- Al-Malah, K., Azzam, M.O.J., Abu-Lail, N.I., 2000. Olive mills effluent (OME) wastewater post-treatment using activated clay. *Separ. Purif. Technol.* 20, 225–234. [https://doi.org/10.1016/S1383-5866\(00\)00114-3](https://doi.org/10.1016/S1383-5866(00)00114-3).
- Alhamed, Y.A., 2009. Adsorption kinetics and performance of packed bed adsorber for phenol removal using activated carbon from dates' stones. *J. Hazard Mater.* 170, 763–770. <https://doi.org/10.1016/j.jhazmat.2009.05.002>.
- Allen, S.J., McKay, G., Khader, K.Y., 1989. Intraparticle diffusion of a basic dye during adsorption onto sphagnum peat. *Environ. Pollut.* 56, 39–50. [https://doi.org/10.1016/0269-7491\(89\)90120-6](https://doi.org/10.1016/0269-7491(89)90120-6).
- Alslaibi, T.M., Abustan, I., Ahmad, M.A., Foul, A.A., 2014. Kinetics and equilibrium adsorption of iron (II), lead (II), and copper (II) onto activated carbon prepared from olive stone waste. *Desalination Water Treat.* 52, 7887–7897. <https://doi.org/10.1080/19443994.2013.833875>.
- Ayawei, N., Ebelegi, A.N., Wankasi, D., 2017. Modelling and interpretation of adsorption isotherms. *J. Chem.* 2017 <https://doi.org/10.1155/2017/3039817>.
- Baccar, R., Bouzid, J., Feki, M., Montiel, A., 2009. Preparation of activated carbon from Tunisian olive-waste cakes and its application for adsorption of heavy metal ions. *J. Hazard Mater.* 162, 1522–1529. <https://doi.org/10.1016/j.jhazmat.2008.06.041>.
- Baccar, R., Blázquez, P., Bouzid, J., Feki, M., Sarrá, M., 2010. Equilibrium, thermodynamic and kinetic studies on adsorption of commercial dye by activated carbon derived from olive-waste cakes. *Chem. Eng. J.* 165, 457–464. <https://doi.org/10.1016/j.cej.2010.09.033>.
- Bansal, R.C., Donnet, J.B., Stoeckli, F., 1998. *Active Carbon*. Dekker, New York.
- Baçaoui, A., Dahbi, A., Yaacoubi, A., Bennouna, C., Maldonado-Hódar, F.J., Rivera-Utrilla, J., Carrasco-Marín, F., Moreno-Castilla, C., 2002. Experimental design to optimize preparation of activated carbons for use in water treatment. *Environ. Sci. Technol.* 36, 3844–3849. <https://doi.org/10.1021/es010305t>.

- Blanchard, G., Maunay, M., Martin, G., 1984. Removal of heavy metals from waters by means of natural zeolites. *Water Res.* 18, 1501–1507. [https://doi.org/10.1016/0043-1354\(84\)90124-6](https://doi.org/10.1016/0043-1354(84)90124-6).
- Brunauer, S., Emmett, P.H., Teller, E., 1938. Adsorption of gases in multimolecular layers. *J. Am. Chem. Soc.* 60, 309–319. <https://doi.org/10.1021/ja01269a023>.
- Cazorla-Amorós, D., Alcañal Iz-Monge, J., De La Casa-Lillo, M.A., Linares-Solano, A., 1998. CO₂ as an adsorptive to characterize carbon molecular sieves and activated carbons. *Langmuir* 14, 4589–4596. <https://pubs.acs.org/sharingguidelines>.
- Conde, E., Moure, A., Domínguez, H., 2017. Recovery of phenols from autohydrolysis liquors of barley husks: kinetic and equilibrium studies. *Ind. Crop. Prod.* 103, 175–184. <https://doi.org/10.1016/j.indcrop.2017.03.048>.
- De Marco, E., Savarese, M., Paduano, A., Sacchi, R., 2007. Characterization and fractionation of phenolic compounds extracted from olive oil mill wastewaters. *Food Chem.* 104, 858–867. <https://doi.org/10.1016/j.foodchem.2006.10.005>.
- Dermeche, S., Nadour, M., Larroche, C., Mouti-Mati, F., Michaud, P., 2013. Olive mill wastes: biochemical characterizations and valorization strategies. *Process Biochem.* 48, 1532–1552. <https://doi.org/10.1016/j.procbio.2013.07.010>.
- Eder, S., Müller, K., Azzari, P., Arcifa, A., Peydayesh, M., Nyström, L., 2021. Mass transfer mechanism and equilibrium modelling of hydroxytyrosol adsorption on olive pit-derived activated carbon. *Chem. Eng. J.* 404, 126519. <https://doi.org/10.1016/j.cej.2020.126519>.
- El-Abbassi, A., Kiai, H., Hafidi, A., 2012. Phenolic profile and antioxidant activities of olive mill wastewater. *Food Chem.* 132, 406–412. <https://doi.org/10.1016/j.foodchem.2011.11.013>.
- El-Sheikh, A.H., Newman, A.P., Said, A.J., Alzawahreh, A.M., Abu-Helal, M.M., 2013. Improving the adsorption efficiency of phenolic compounds into olive wood biosorbents by pre-washing with organic solvents: equilibrium, kinetic and thermodynamic aspects. *J. Environ. Manag.* 118, 1–10. <https://doi.org/10.1016/j.jenvman.2013.01.009>.
- Fajardo, A.S., Rodrigues, R.F., Martins, R.C., Castro, L.M., Quinta-Ferreira, R.M., 2015. Phenolic wastewaters treatment by electrocoagulation process using Zn anode. *Chem. Eng. J.* 275, 331–341. <https://doi.org/10.1016/j.cej.2015.03.116>.
- Fierro, V., Torné-Fernández, V., Montañé, D., Celzard, A., 2008. Adsorption of phenol onto activated carbons having different textural and surface properties. *Microporous Mesoporous Mater.* 111, 276–284. <https://doi.org/10.1016/j.micromeso.2007.08.002>.
- Frascardi, D., Bacca, A.E.M., Zama, F., Bertin, L., Fava, F., Pinelli, D., 2016. Olive mill wastewater valorisation through phenolic compounds adsorption in a continuous flow column. *Chem. Eng. J.* 283, 293–303. <https://doi.org/10.1016/j.cej.2015.07.048>.
- Frascardi, D., Rubertelli, G., Arous, F., Ragini, A., Bresciani, L., Arzu, A., Pinelli, D., 2019. Valorisation of olive mill wastewater by phenolic compounds adsorption: development and application of a procedure for adsorbent selection. *Chem. Eng. J.* 360, 124–138. <https://doi.org/10.1016/j.cej.2018.11.188>.
- Galiatsatou, P., Metaxas, M., Arapoglou, D., Kasselouri-Rigopoulou, V., 2002. Treatment of olive mill waste water with activated carbons from agricultural by-products. *Waste Manag.* 22, 803–812. [https://doi.org/10.1016/S0956-053X\(02\)00055-7](https://doi.org/10.1016/S0956-053X(02)00055-7).
- García-Araya, J.F., Beltrán, F.J., Álvarez, P., Masa, F.J., 2003. Activated carbon adsorption of some phenolic compounds present in agroindustrial wastewater. *Adsorption* 9, 107–115. <https://doi.org/10.1023/A:1024228708675>.
- García-Castello, E., Cassano, A., Criscoli, A., Conidi, C., Drioli, E., 2010. Recovery and concentration of polyphenols from olive mill wastewaters by integrated membrane system. *Water Res.* 44, 3883–3892. <https://doi.org/10.1016/j.watres.2010.05.005>.
- Ghouma, I., Jeguirim, M., Sager, U., Limousy, L., Bennici, S., Däuber, E., Asbach, C., Ligotski, R., Schmidt, F., Ouederni, A., 2017. The potential of activated carbon made of agro-industrial residues in NOx immissions abatement. *Energies* 10, 1508. <https://doi.org/10.3390/en10101508>.
- Hamadneh, I., Abu-Zurayk, R.A., Al-Dujaili, A.H., 2020. Removal of phenolic compounds from aqueous solution using MgCl₂-impregnated activated carbons derived from olive husk: the effect of chemical structures. *Water Sci. Technol.* 81, 2351–2367. <https://doi.org/10.2166/wst.2020.297>.
- Hazzaa, R., Hussein, M., 2015. Adsorption of cationic dye from aqueous solution onto activated carbon prepared from olive stones. *Environ. Technol. Innovat.* 4, 36–51. <https://doi.org/10.1016/j.eti.2015.04.002>.
- Ho, Y.S.S., McKay, G., 1999. Pseudo-second order model for sorption processes. *Process Biochem.* 34. <https://doi.org/10.1021/acs.oprd.7b00090>, 451–465.
- Hodaifa, G., Ochando-Pulido, J.M., Ben Driss Alami, S., Rodríguez-Vives, S., Martínez-Ferez, A., 2013. Kinetic and thermodynamic parameters of iron adsorption onto olive stones. *Ind. Crop. Prod.* 49, 526–534. <https://doi.org/10.1016/j.indcrop.2013.05.039>.
- Jeguirim, M., Belhachechi, M., Limousy, L., Bennici, S., 2018. Adsorption/reduction of nitrogen dioxide on activated carbons: textural properties versus surface chemistry – a review. *Chem. Eng. J.* 347, 493–504. <https://doi.org/10.1016/j.cej.2018.04.063>.
- Justino, C.I., Duarte, K., Loureiro, F., Pereira, R., Antunes, S.C., Marques, S.M., Gonçalves, F., Rocha-Santos, T.A.P., Freitas, A.C., 2009. Toxicity and organic content characterization of olive oil mill wastewater undergoing a sequential treatment with fungi and photo-Fenton oxidation. *J. Hazard Mater.* 172, 1560–1572. <https://doi.org/10.1016/j.jhazmat.2009.08.028>.
- Kapellakis, I.E., Tzarakis, K.P., Crowther, J.C., 2008. Olive oil history, production and by-product management. *Rev. Environ. Sci. Biotechnol.* 7, 1–26. <https://doi.org/10.1007/s11157-007-9120-9>.
- Kilic, M.Y., Abdelraheem, W.H., He, X., Kestioglu, K., Dionysiou, D.D., 2019. Photochemical treatment of tyrosol, a model phenolic compound present in olive mill wastewater, by hydroxyl and sulfate radical-based advanced oxidation processes (AOPs). *J. Hazard Mater.* 367, 734–742. <https://doi.org/10.1016/j.jhazmat.2018.06.062>.
- Kumar, A., Kumar, S., Kumar, S., 2003. Adsorption of resorcinol and catechol on granular activated carbon: equilibrium and kinetics. *Carbon N. Y.* 41, 3015–3025. [https://doi.org/10.1016/S0008-6223\(03\)00431-7](https://doi.org/10.1016/S0008-6223(03)00431-7).
- Lagergren, S., 1898. About the theory of so-called adsorption of soluble substances. *K. -Sven. Vetenskapsakademiens Handl.* 24, 1–39.
- Li, Z., Sellaoui, L., Luiz Dotto, G., Bonilla-Petriciolet, A., Ben Lamine, A., 2019. Understanding the adsorption mechanism of phenol and 2-nitrophenol on a biopolymer-based biochar in single and binary systems via advanced modeling analysis. *Chem. Eng. J.* 371, 1–6. <https://doi.org/10.1016/j.cej.2019.04.035>.
- Macedo, E., Santos, M.S.F., Maldonado-Hódar, F.J., Alves, A., Madeira, L.M., 2018. Insights on carbonaceous materials tailoring for effective removal of the anticancer drug 5-fluorouracil from contaminated waters. *Ind. Eng. Chem. Res.* 57, 3932–3940. <https://doi.org/10.1021/acs.iecr.7b05145>.
- Michailof, C., Stavropoulos, G.G., Panayiotou, C., 2008. Enhanced adsorption of phenolic compounds, commonly encountered in olive mill wastewaters, on olive husk derived activated carbons. *Bioresour. Technol.* 99, 6400–6408. <https://doi.org/10.1016/j.biortech.2007.11.057>.
- Mohd Din, A.T., Hameed, B.H., Ahmad, A.L., 2009. Batch adsorption of phenol onto physicochemical-activated coconut shell. *J. Hazard Mater.* 161, 1522–1529. <https://doi.org/10.1016/j.jhazmat.2008.05.009>.
- Morales-Torres, S., Silva, A.M.T., Pérez-Cadenas, A.F., Faria, J.L., Maldonado-Hódar, F.J., Figueiredo, J.L., Carrasco-Marín, F., 2010a. Wet air oxidation of trinitrophenol with activated carbon catalysts: effect of textural properties on the mechanism of degradation. *Appl. Catal. B Environ.* 100, 310–317. <https://doi.org/10.1016/j.apcatb.2010.08.007>.
- Morales-Torres, S., Maldonado-Hódar, F.J., Pérez-Cadenas, A.F., Carrasco-Marín, F., 2010b. Design of low-temperature Pt-carbon combustion catalysts for VOC's treatments. *J. Hazard Mater.* 183, 814–822. <https://doi.org/10.1016/j.jhazmat.2010.07.100>.
- Moreno-Castilla, C., Rivera-Utrilla, J., López-Ramón, M.V., Carrasco-Marín, F., 1995. Adsorption of some substituted phenols on activated carbons from a bituminous coal. *Carbon N. Y.* 33, 845–851. [https://doi.org/10.1016/0008-6223\(94\)00182-Y](https://doi.org/10.1016/0008-6223(94)00182-Y).
- Moreno-Castilla, C., Pérez-Cadenas, A.F., Maldonado-Hódar, F.J., Carrasco-Marín, F., Fierro, J.L.G., 2003. Influence of carbon-oxygen surface complexes on the surface acidity of tungsten oxide catalysts supported on activated carbons. *Carbon N. Y.* 41, 1157–1167. [https://doi.org/10.1016/S0008-6223\(03\)00023-X](https://doi.org/10.1016/S0008-6223(03)00023-X).
- Neimark, A.V., Lin, Y., Ravikovitch, P.I., Thommes, M., 2009. Quenched solid density functional theory and pore size analysis of micro-mesoporous carbons. *Carbon N. Y.* 47, 1617–1628. <https://doi.org/10.1016/j.carbon.2009.01.050>.
- Newcombe, G., Hayes, R., Drikas, M., 1993. Granular activated carbon: importance of surface properties in the adsorption of naturally occurring organics. *Coll. Surfaces A Physicochem. Eng. Asp.* 78, 65–71. [https://doi.org/10.1016/0927-7757\(93\)80311-2](https://doi.org/10.1016/0927-7757(93)80311-2).
- Niaounakis, M., Halvadakis, C.P., 2006. Characterization of olive processing waste. In: *Waste Manag. Ser.*, second ed. Elsevier Ltd, Amsterdam, pp. 23–64. [https://doi.org/10.1016/S0713-2743\(06\)80004-8](https://doi.org/10.1016/S0713-2743(06)80004-8).
- Ochando-Pulido, J.M., Pimentel-Moral, S., Verardo, V., Martínez-Ferez, A., 2017. A focus on advanced physico-chemical processes for olive mill wastewater treatment. *Separ. Purif. Technol.* 179, 161–174.
- Ochando-Pulido, J.M., Corpas-Martínez, J.R., Vellido-Perez, J.A., Martínez-Ferez, A., 2020. Optimization of polymeric nanofiltration performance for olive-oil-washing wastewater phenols recovery and reclamation. *Separ. Purif. Technol.* 236, 116261. <https://doi.org/10.1016/j.seppur.2019.116261>.
- Paraskeva, P., Diamadopoulos, E., 2006. Technologies for olive mill wastewater (OMW) treatment: a review. *J. Chem. Technol. Biotechnol.* 81, 1475–1485.
- Petrella, A., Spasiano, D., Acquafredda, P., De Vietro, N., Ranieri, E., Cosma, P., Rizzi, V., Petruzzelli, V., Petruzzelli, D., 2018. Heavy metals retention (Pb(II), Cd(II), Ni(II)) from single and multimetal solutions by natural biosorbents from the olive oil milling operations. *Process Saf. Environ. Protect.* 114, 79–90. <https://doi.org/10.1016/j.psep.2017.12.010>.
- Pholosi, A., Naidoo, E.B., Ofomaja, A.E., 2020. Intraparticle diffusion of Cr(VI) through biomass and magnetite coated biomass: a comparative kinetic and diffusion study. *S. Afr. J. Chem. Eng.* 32, 39–55. <https://doi.org/10.1016/j.sajce.2020.01.005>.
- Rivera-Utrilla, J., Moreno-Castilla, C., Utrera-Hidalgo, E., Carrasco-Marín, F., 1993. Removal of tannic acid from aqueous solutions by activated carbons. *Chem. Eng. J.* 52, 37–39. [https://doi.org/10.1016/0300-9467\(93\)80040-U](https://doi.org/10.1016/0300-9467(93)80040-U).
- Rouquerol, J., Rouquerol, F., Llewellyn, P., Maurin, G., Sing, K.S.W., 2013. *Adsorption by Powders and Porous Solids: Principles, Methodology and Applications*, second ed. Academic Press, Oxford. <https://doi.org/10.1016/C2010-0-66232-8>.
- Salleh, M.A.M., Mahmoud, D.K., Karim, W.A.W.A., Idris, A., 2011. Cationic and anionic dye adsorption by agricultural solid wastes: a comprehensive review. *Desalination* 280, 1–13. <https://doi.org/10.1016/j.desal.2011.07.019>.
- Seader, J.D., Henley, E.J., Keith Roper, D., 2010. *Separation Process Principles*, third ed. John Wiley Incorporated, Hoboken, NJ.
- Soto, M.L., Moure, A., Domínguez, H., Parajó, J.C., 2011. Recovery, concentration and purification of phenolic compounds by adsorption: a review. *J. Food Eng.* 105, 1–27. <https://doi.org/10.1016/j.jfoodeng.2011.02.010>.
- Srivastava, V.C., Mall, I.D., Mishra, I.M., 2008. Adsorption of toxic metal ions onto activated carbon. Study of sorption behaviour through characterization and kinetics. *Chem. Eng. Process. Process Intensif.* 47, 1269–1280. <https://doi.org/10.1016/j.ccep.2007.04.006>.
- Stasinakis, A.S., Elia, I., Petalas, A.V., Halvadakis, C.P., 2008. Removal of total phenols from olive-mill wastewater using an agricultural by-product, olive pomace. *J. Hazard Mater.* 160, 408–413. <https://doi.org/10.1016/j.jhazmat.2008.03.012>.

- Stavropoulos, G.G., Zabaniotou, A.A., 2005. Production and characterization of activated carbons from olive-seed waste residue. *Microporous Mesoporous Mater.* 82, 79–85. <https://doi.org/10.1016/j.micromeso.2005.03.009>.
- Stoeckli, F., Guillot, A., Slasli, A., Hugi-Cleary, D., 2002. Microporosity in carbon blacks. *Carbon N. Y.* 40, 211–215. [https://doi.org/10.1016/S0008-6223\(01\)00176-2](https://doi.org/10.1016/S0008-6223(01)00176-2).
- Stoller, M., Azizova, G., Mammadova, A., Vilardi, G., Di Palma, L., Chianese, A., 2016. Treatment of olive oil processing wastewater by ultrafiltration, nanofiltration, reverse osmosis and biofiltration. *Chem. Eng. Trans.* 47, 409–414. <https://doi.org/10.3303/CET1647069>.
- Sun, J., Liu, X., Zhang, F., Zhou, J., Wu, J., Alsaedi, A., Hayat, T., Li, J., 2019. Insight into the mechanism of adsorption of phenol and resorcinol on activated carbons with different oxidation degrees. *Coll. Surfaces A Physicochem. Eng. Asp.* 563, 22–30. <https://doi.org/10.1016/j.colsurfa.2018.11.042>.
- Thommes, M., Kaneko, K., Neimark, A.V., Olivier, J.P., Rodriguez-Reinoso, F., Rouquerol, J., Sing, K.S.W., 2015. Physisorption of gases, with special reference to the evaluation of surface area and pore size distribution (IUPAC Technical Report). *Pure Appl. Chem.* 87, 1051–1069. <https://doi.org/10.1515/pac-2014-1117>.
- Toor, M., Jin, B., 2012. Adsorption characteristics, isotherm, kinetics, and diffusion of modified natural bentonite for removing diazo dye. *Chem. Eng. J.* 187, 79–88. <https://doi.org/10.1016/j.cej.2012.01.089>.
- Tundis, R., Conidi, C., Loizzo, M.R., Sicari, V., Romeo, R., Cassano, A., 2021. Concentration of bioactive phenolic compounds in olive mill wastewater by direct contact membrane distillation. *Molecules* 26, 1808. <https://doi.org/10.3390/molecules26061808>.
- Víctor-Ortega, M.D., Ochando-Pulido, J.M., Airado-Rodríguez, D., Martínez-Ferez, A., 2016. Comparison between different ion exchange resins combinations for final treatment of olive mill effluent. *Separ. Purif. Technol.* 158, 374–382. <https://doi.org/10.1016/j.seppur.2015.12.041>.
- Viegas, R.M.C., Campinas, M., Costa, H., Rosa, M.J., 2014. How do the HSDM and Boyd's model compare for estimating intraparticle diffusion coefficients in adsorption processes. *Adsorption* 20, 737–746. <https://doi.org/10.1007/s10450-014-9617-9>.
- Wanassi, B., Ben Hariz, I., Ghimbeu, C.M., Vaultot, C., Ben Hassen, M., Jeguirim, M., 2017. Carbonaceous adsorbents derived from textile cotton waste for the removal of Alizarin S dye from aqueous effluent: kinetic and equilibrium studies. *Environ. Sci. Pollut. Res.* 24, 10041–10055. <https://doi.org/10.1007/s11356-017-8410-1>.
- Wang, J., Guo, X., 2020. Adsorption kinetic models: physical meanings, applications, and solving methods. *J. Hazard Mater.* 390, 122156. <https://doi.org/10.1016/j.jhazmat.2020.122156>.
- Wang, W., Gong, Q., Chen, Z., Wang, W.D., Huang, Q., Song, S., Chen, J., Wang, X., 2019. Adsorption and competition investigation of phenolic compounds on the solid-liquid interface of three-dimensional foam-like graphene oxide. *Chem. Eng. J.* 378, 122085. <https://doi.org/10.1016/j.cej.2019.122085>.
- Weber Jr., W.J., Morris, J.C., 1963. Kinetics of adsorption on carbon from solution. *J. Sanit. Eng. Div.* 89, 31–59. <https://doi.org/10.1061/JSEDAI.0000430>.
- Yangui, A., Njimou, J.R., Cicci, A., Bravi, M., Abderrabba, M., Chianese, A., 2017. Competitive adsorption, selectivity and separation of valuable hydroxytyrosol and toxic phenol from olive mill wastewater. *J. Environ. Chem. Eng.* 5, 3581–3589. <https://doi.org/10.1016/j.jece.2017.06.037>.
- Zagklis, D.P., Vavouraki, A.I., Kornaros, M.E., Paraskeva, C.A., 2015. Purification of olive mill wastewater phenols through membrane filtration and resin adsorption/desorption. *J. Hazard Mater.* 285, 69–76. <https://doi.org/10.1016/j.jhazmat.2014.11.038>.